**Aalto University**
**School of Chemical Technology**

**School of Chemical Technology**
**Degree Programme of Materials Science and Engineering**

**Miamari Aaltonen**

# CHARACTERIZATION OF ADHERENT ANODE SLIMES IN COPPER ELECTROREFINING

**Master's thesis for the degree of Master of Science in Technology submitted for inspection, Espoo, 12.11.2014.**

**Supervisor** **Professor Olof Forsén**

**Instructor** **D.Sc. Jari Aromaa**

Aalto University
School of Chemical
Technology

Aalto University, P.O. BOX 11000, 00076 AALTO
www.aalto.fi
**Abstract of master's thesis**

| | | |
|---|---|---|
| **Author** Miamari Aaltonen | | |
| **Title of thesis** Characterization of adherent anode slimes in copper electrorefining | | |
| **Department** Materials Science and Engineering | | |
| **Professorship** Corrosion and Hydrometallurgy | | **Code of Professorship** MT-85 |
| **Thesis supervisor** Professor Olof Forsén | | |
| **Thesis advisor / Thesis examiner** D.Sc. Jari Aromaa | | |
| **Date** 12.11.2014 | **Number of pages** 59 | **Language** English |

The goals of the thesis were to produce information of the adherent anode slimes and to examine the effects that anode composition and process parameters have on them. In the experimental section, 31 adherent anode slime samples were examined with the help of moisture content determination, settling tests, particle size distribution measurements, chemical analysis, x-ray diffraction and scanning electron microscopy. Corresponding anode lug samples were examined with the help of chemical analysis and optical microscopy.

From the produced analysis data, correlations were difficult to establish. A connection was found between the chemical and XRD analysis results of nickel, which is also in line with the information found in literature. The process parameter data was not compared with the analysis results due to difficulties in connecting the sample with the corresponding data.

Based on the analysis results, adherent anode slime sampling and some of the experimental methods need to be developed further. Also, information can still be extracted from the data produced with the help of more advanced data analysis.

**Keywords** copper electrorefining, adherent anode slimes, nickel, settling, particle size distribution, chemical analysis, SEM, XRD, optical microscopy

Aalto-yliopisto
Kemian tekniikan korkeakoulu

Aalto-yliopisto, PL 11000, 00076 AALTO
www.aalto.fi
**Diplomityön tiivistelmä**

| | | |
|---|---|---|
| **Tekijä** Miamari Aaltonen | | |
| **Työn nimi** Anodin pinnassa kiinni pysyvän anodiliejun karakterisointi kuparin raffinointielektrolyysissä | | |
| **Laitos** Materiaalitekniikka | | |
| **Professuuri** Korroosio ja hydrometallurgia | | **Professuurikoodi** MT-85 |
| **Valvoja** Professori Olof Forsén | | |
| **Ohjaaja** TkT Jari Aromaa | | |
| **Päivämäärä** 12.11.2014 | **Sivumäärä** 59 | **Kieli** Englanti |

Työn tavoitteina on tuottaa tietoa anodin pinnassa kiinni pysyvän anodiliejun ominaisuuksista sekä tutkia, miten anodin koostumus sekä prosessiparametrit niihin vaikuttavat. Anodin pinnassa kiinni pysyvän anodiliejun ominaisuuksiin liittyvää tietoa tuotettiin 31 liejunäytteen kosteusprosenttimäärityksen, laskeutuskokeiden, partikkelikokojakauma-analyysien, kemiallisten analyysien, XRD-analyysien sekä SEM-kuvien avulla. Liejunäytteitä vastaavat anodinäytteet tutkittiin kemiallisen analyysin ja optisen mikroskopian avulla.

Eri analyysitulosten välisiä korrelaatioita oli vaikea löytää. Ainoa merkittävä yhteys ilmeni nikkelin kemiallisten ja XRD-analyysien välillä. Löytynyt yhteys mainitaan myös kirjallisuuslähteissä. Prosessiparametrien vaikutusta liejun analyysituloksiin ei lopulta tutkittu johtuen hankaluuksista prosessiparametridatan yhdistämisessä tiettyyn näytteeseen.

Analyysitulosten perusteella anodin pinnassa kiinni pysyvän anodiliejun näytteenottoa sekä joitakin kokeellisia menetelmiä tulee vielä kehittää. Analyysituloksista lienee myös mahdollista löytää lisää korrelaatioita kehittyneempien data-analyysien avulla.

**Avainsanat** kuparin raffinointielektrolyysi, anodin pinnassa kiinni pysyvä anodilieju, nikkeli, laskeutus, partikkelikokojakauma, kemiallinen analyysi, SEM, XRD, optinen mikroskopia

# Preface

The research for this thesis was done at Aalto University School of Chemical Technology, department of Materials Science and Engineering, in the research group of Corrosion and Hydrometallurgy, during February - October, 2014. The thesis is a part of FIMECC's (Finnish Metals and Engineering Competence Cluster) SIMP (System Integrated Metal Production) programme and was done in co-operation with Boliden Pori electrorefinery, Boliden Harjavalta and Outotec Research Center, Pori.

I express my sincere gratitude to Professor Olof Forsén, the thesis supervisor, and to D.Sc. Jari Aromaa, the thesis advisor, who have offered both help and valuable advice along the way.

I would also like to thank the staff members of the research group of Corrosion and Hydrometallurgy for their help and support during the making of the thesis. A sincere thanks goes also to the staff members of the department's workshop and to the helpful members of the research groups of Mechanical Processing and Recycling, of Metallurgical Thermodynamics and Modelling, of Materials Processing and Powder Metallurgy and of Advanced and Functional Materials for their shared expertise and co-operation.

A special thanks goes to Elina Niemi from Boliden Pori electrorefinery, to Noora Aro-Koivisto from Outotec Research Center, Pori and to Petri Latostenmaa from Boliden Harjavalta for the knowledge they have shared and for the interest they have taken in my work.

Lastly, a warm thank you to my dear family and friends for the support and encouragement they have given me during the thesis making process.

# Contents

# 1 Introduction

In order to produce high purity copper from copper ores, the ores need to be concentrated, smelted, converted and refined. Copper ores typically contain from 0.5 % to 2 % copper. In the copper ores, the most common copper containing minerals are chalcopyrite ($CuFeS_2$) and chalcocite ($Cu_2S$). The concentrating of these $Cu-Fe-S$ and $Cu-S$ minerals consists of crushing and grinding the ores into smaller particles and of froth flotation. After the froth flotation, the copper concentrate contains around 30 % of copper. The matte smelting of the copper concentrate produces a molten sulfide matte that contains from 45 % to 75 % copper. (Schlesinger et al. 2011.)

After smelting, the copper matte is converted. The converting of the copper matte consists of the removal of iron and sulfur by oxidation. After converting, the produced blister copper contains around 99 % of copper. The blister copper is then fire refined and electrorefined. (Schlesinger et al. 2011.)

The fire refining of the molten blister copper consists of sulfur and oxygen removal. The fire refined molten copper contains around 0.003 % of sulfur and 0.16 % of oxygen and is cast into anodes. The impure anode copper is electrorefined in order to achieve high purity copper. In the electrorefining of copper, the anode dissolves into the electrolyte and pure copper is electrodeposited on the cathode. The copper content of the electrorefined cathode copper is greater than 99.997 %. (Schlesinger et al. 2011.)

The impure anode copper contains both base and noble metals as impurities. The base metals dissolve from the anode with copper and report to the electrolyte. The noble metals do not dissolve and form anode slimes. The anode slimes formed can either adhere to the anode surface or fall to the bottom of the refining cell (Davenport et al. 2002). The formation of floating slimes is also possible (Moats & Hiskey, 2010). In this thesis, the anode slimes that adhere to the anode's surface are referred to as adherent anode slimes.

The formation of adherent anode slimes can inhibit the dissolution of the anodes. If the dissolution reaction is completely inhibited, the anode passivates (Moats & Hiskey, 2010). The anode passivation causes the process to be inefficient (Cheng & Hiskey, 1996), i.e. the anode passivation can cause losses in the production capacity, increased power costs and decreased cathode quality (Moats & Hiskey, 2010).

As a hypothesis of the thesis, anode impurities and microstructure can affect the amount

and adherence of the adherent anode slimes. The impurities of interest in the thesis are oxygen ($O_2$), silver (Ag), nickel (Ni), arsenic (As), antimony (Sb), bismuth (Bi), lead (Pb), selenium (Se) and tellurium (Te). The known tendencies are that lead increases the amount of adherent anode slimes, whereas arsenic decreases both their amount and adherence. In addition to the effects of the anode impurities on the formation of adherent anode slimes, also the effects of the electrorefining process parameters will be briefly discussed.

The beginning of the thesis presents significant data found in literature. After the literature review, the research methods and their results are presented. The research methods include moisture content determination, settling tests, particle size distribution measurements, x-ray diffraction (XRD), scanning electron microscopy (SEM) and optical microscopy. Optical microscopy will be used in anode microstructure characterization whereas the other research methods will be used in the characterization of the adherent anode slimes.

Finally, conclusions are drawn and recommendations for future studies are made. From the data produced, correlations were difficult to establish. However, a connection was found between the chemical and XRD analysis results of nickel, which is in line with the information found in literature. The thesis is a part of FIMECC's SIMP programme.

# 2 Anodes and adherent anode slimes

This section presents the significant anode and adherent anode slime related data found in literature. The following subchapters present in more detail the copper electorefining process and different factors affecting the adherent anode slimes.

## 2.1 The electrorefining of copper

In the electrorefining process, copper is dissolved electrochemically from the impure copper anode into the electrolyte and then electrodeposited as pure copper. The used electrolyte typically contains copper sulphate ($CuSO_4$) and sulphuric acid ($H_2SO_4$). (Schlesinger et al. 2011.) Table 1 shows the global average electrolyte compositions from the tank house data of Copper 2003, 2007, 2010 and 2013 (Moats et al. 2013).

Table 1: The average electrolyte compositions globally, adapted from (Moats et al. 2013).

| Average composition (g/l) | 2003 | 2007 | 2010 | 2013 |
|---|---|---|---|---|
| $H_2SO_4$ | 175 | 172 | 178 | 173 |
| Cu | 48 | 48 | 48 | 49 |
| Ni | 10.8 | 11.4 | 12.8 | 13.0 |
| As | 5.5 | 6.9 | 6.9 | 5.5 |
| Sb | 0.3 | 0.3 | 0.3 | 0.3 |
| Bi | 0.2 | 0.2 | 0.3 | 0.2 |

The impure anodes usually have a purity of 98.5-99.5 % copper. Industrial copper anodes are typically large, about 1 $m^2$, and thin (4-5 cm). The mass of an anode is between 300-400 kg. (Schlesinger et al. 2011.) The anodes are cast and have therefore an air side and a mould side. A copper anode is presented in figure 1. Nowadays many copper electrorefineries use stainless steel blanks as cathodes (figure 1). The cathodes are usually flat, cold- and bright-rolled 316L stainless steel and about 3 mm thick. The purity of the electrodeposited copper on the cathodes is greater than 99.997 %. Schlesinger et al. 2011.)

A flow sheet of the electrorefining process of copper is presented in figure 2. The electrorefining process starts with the loading of the electrodes into the cell. The anodes and cathodes are placed evenly in the electrolyte filled cell, about 50 mm apart from the cen-

terline, in order to achieve an even current distribution to all of them. The electrolyte continuously enters the cells from their bottom end and leaves from the other end, into an electrolyte collecting system. (Schlesinger et al. 2011.) The global average cell voltages, cathode current densities and current efficiencies from the tank house data of Copper 2003, 2007, 2010 and 2013 (Moats et al. 2013) are presented in table 2.

Table 2: The average cell voltages, cathode current densities and current efficiencies globally, adapted from (Moats et al. 2013).

| Average | 2003 | 2007 | 2010 | 2013 |
|---|---|---|---|---|
| Cell voltage (mV) | 308 | 315 | 314 | 338 |
| Cathode current density (A/m$^2$) | 283 | 284 | 298 | 310 |
| Current efficiency (%) | 95.3 | 95.6 | 96.1 | 96.3 |

The electrorefining process ends with the unloading of the dissolved anodes. The anodes are removed once they are down to 15-20 % of their original mass, which usually takes about 21 days. The anode scrap is washed free of slimes and processed into new anodes. (Schlesinger et al. 2011.) Figure 3 shows adherent anode slime covered scrap anodes on their way to be washed, in the Boliden Pori electrorefinery. The cathodes are removed sooner than the anodes, typically after 7-10 days. During this time, around 50-80 kg of pure copper is electrodeposited onto them. The pure copper is machine-stripped from the stainless steel blanks. (Schlesinger et al. 2011.)

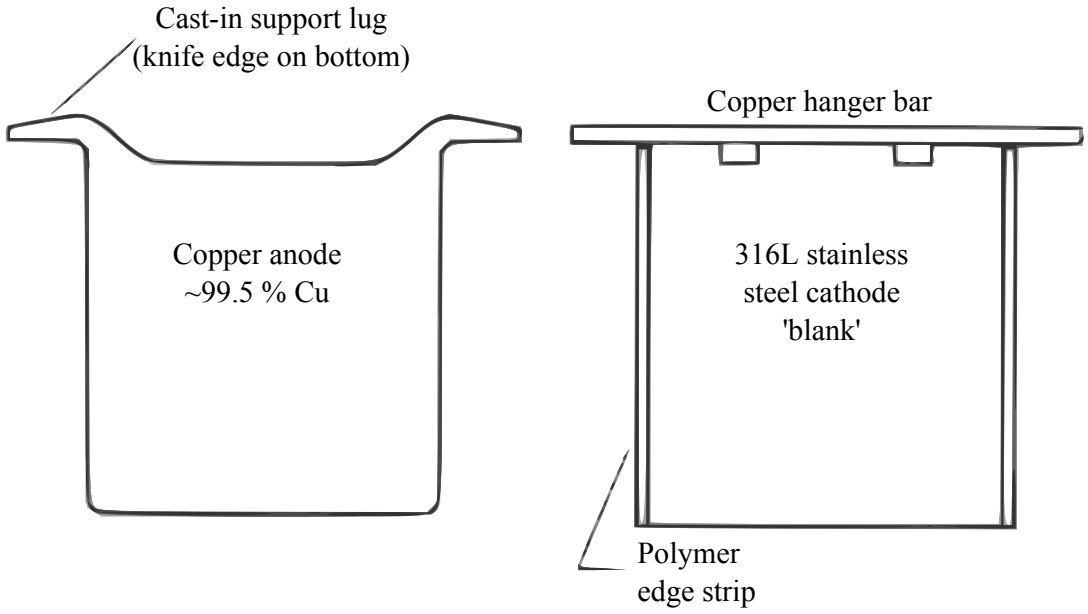


Figure 1: On the left, a copper anode and on the right, a stainless steel cathode, adapted from (Davenport et al. 2002).

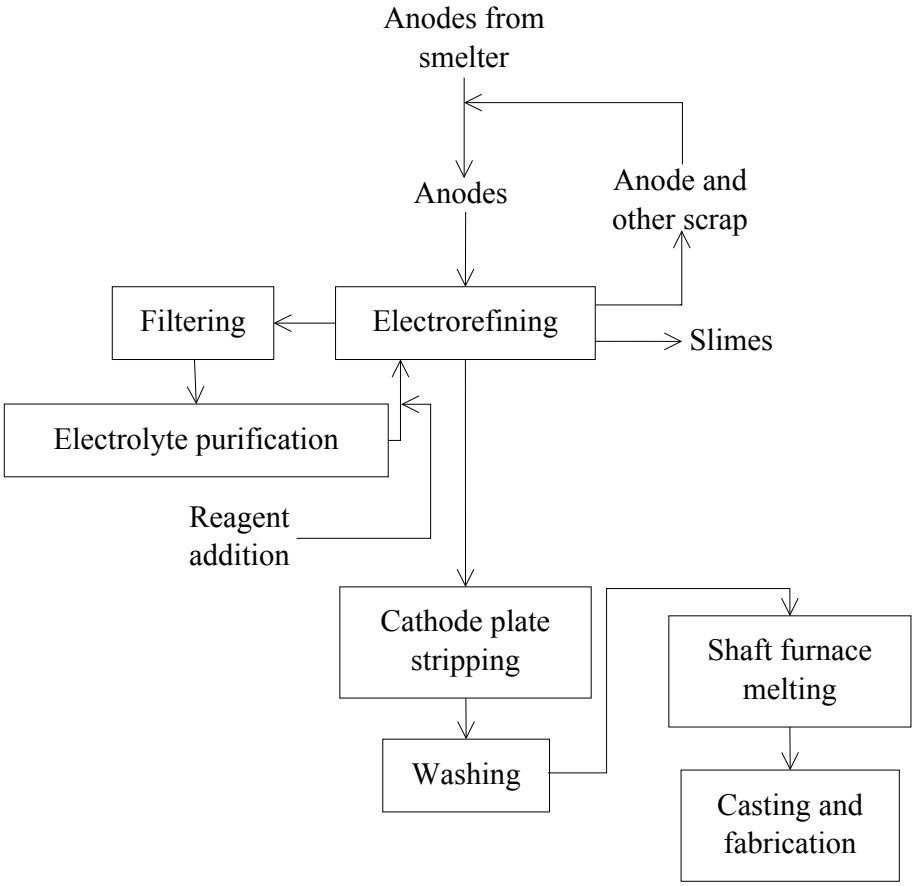


Figure 2: A flowsheet of the electrorefining process of copper, adapted from (Davenport et al. 2002).

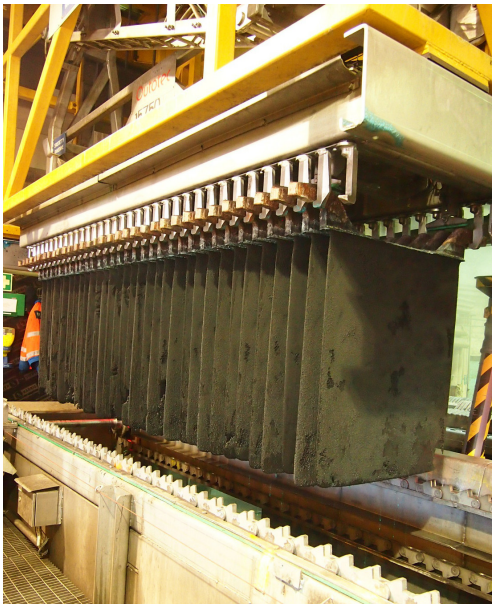

Figure 3: Adherent anode slime covered scrap anodes on their way to be washed, in the Boliden Pori electorefinery. © Research group of Corrosion and Hydrometallurgy (CORR)

## 2.2 Anode composition and microstructure

The impurity elements of anode copper can be divided into two groups: insoluble and soluble impurity elements. Furthermore, the soluble elements can either remain dissolved in the electrolyte or precipitate once they get into contact with the electrolyte. Insoluble impurities span the elements nobler than copper, which remain unchanged and form anode slimes. Soluble impurities are the elements less noble than copper, which dissolve in the electrolyte. An example of a soluble impurity element that reprecipitates after dissolution is lead (Pb). The dissolution behavior of different anode impurities will be discussed in more detail in subchapter 2.3 Anode slime formation.

Table 3 shows the global average compositions of copper anodes from the tank house data of Copper 2003, 2007, 2010 and 2013 (Moats et al. 2013). Based on the data of the table, oxygen (O), nickel (Ni), lead, silver (Ag) and arsenic (As) are the main anode impurities. The anode impurities can form a solid solution with copper or discrete inclusions, which are usually located along the copper grain boundaries. In the following subchapters, some of the anode impurities and the species that they occur in are discussed more thoroughly. Table 4 presents a summary of the different impurity species found in the copper anodes. In table 4, the dominant and minor phases of copper are also included.

Table 3: The average compositions of copper anodes globally, adapted from (Moats et al. 2013).

| Element (Concentration) | 2003 | 2007 | 2010 | 2013 |
|---|---|---|---|---|
| Cu (%) | 99.3 | 99.2 | 99.3 | 99.3 |
| O (ppm) | 1580 | 1630 | 1630 | 1460 |
| Ni (ppm) | 1370 | 1410 | 1480 | 2040 |
| Pb (ppm) | 1000 | 1060 | 1140 | 1170 |
| Ag (ppm) | 810 | 850 | 840 | 750 |
| As (ppm) | 790 | 930 | 1010 | 890 |
| Se (ppm) | 350 | 340 | 390 | 400 |
| Sb (ppm) | 280 | 240 | 300 | 350 |
| Bi (ppm) | 130 | 130 | 200 | 180 |
| Te (ppm) | 90 | 100 | 130 | 110 |
| Fe (ppm) | 60 | 40 | 30 | 60 |
| Au (ppm) | 40 | 40 | 60 | 30 |
| S (ppm) | 40 | 30 | 30 | 30 |

Table 4: The anode impurities, adapted from (Chen & Dutrizac, 1989a; 1990b; 1993; Larouche, 2001.)

| Element | Dominant phases | Minor phases |
|---|---|---|
| Cu | Metallic matrix | $Cu_2O$<br>$Cu_2$(Se,Te)<br>Complex oxides |
| O | $Cu_2O$ | NiO<br>Complex oxides |
| Ag | Cu-solid solution | $Cu_2$(Se,Te)<br>Complex oxides |
| Ni | Cu-solid solution | NiO<br>Complex oxides<br>NiO<br>$NiFe_2O_4$<br>Cu−Ni−Fe oxide<br>Kupferglimmer |
| As | Complex oxides | Cu-solid solution |
| Sb | Complex oxides | Cu-solid solution |
| Bi | Complex oxides | Cu-solid solution |
| Pb | Complex oxides | Cu-solid solution |
| Se | $Cu_2$(Se,Te) | |
| Te | $Cu_2$(Se,Te) | |

### 2.2.1 Oxygen

Oxygen is a significant impurity in the copper anodes. Depending on the impurity content of the anode, it forms different oxides ($Cu_2O$, NiO, $As_2O_3$, $Sb_2O_3$ and $Bi_2O_3$) (Möller et al. 2010). Oxygen is also present in various complex oxides (Chen & Dutrizac, 1990b).

An important oxygen containing species in the anodes is cuprous oxide ($Cu_2O$). The $Cu_2O$ inclusions can occur either as free grains or together with other species, such as copper selenide ($Cu_2$(Se,Te)), nickel oxide (NiO) or different Cu−Pb−As−Sb−Bi oxides (figure 4). Some $Cu_2O$ can also be present in Cu−$Cu_2O$ texture between copper grains. The $Cu_2O$ particles have a spheroidal shape and are between $< 1$ to 15 µm in size. (Chen & Dutrizac, 1990b.)

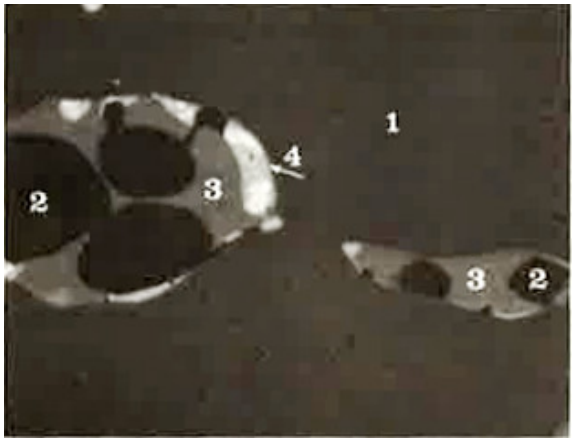


Figure 4: Backscattered electron (BSE) image of a polished copper anode, showing inclusions along the grain boundaries. 1: Copper 2: $Cu_2O$ 3: $Cu_2$(Se,Te) 4: Cu−Pb−As−Sb−Bi oxide. (Chen & Dutrizac, 1990b.)

### 2.2.2 Nickel

According to Chen and Hiskey (1990a), the copper matrix is always the main nickel carrier in anode copper. The research done by Forsén and Lilius (1987) shows that nickel remains in solid solution in the copper matrix at all oxygen contents, if the nickel content of the anode is 0.25 wt-% or less. In their research, Chen and Dutrizac (1989b; 1990a) found out that nickel forms a solid solution with copper in anodes that have a nickel content of less than 0.3 wt-%.

In the research of Chen and Dutrizac (1990a), anodes containing 1100-1500 ppm oxygen and over 0.3 wt-% nickel, more than 85 % of the nickel stayed in solid solution with copper and in addition, nickel oxide (NiO) formed. In the case of low oxygen content (0.1 wt-%) anodes, NiO is only formed with nickel contents higher than 0.32 wt-%. With higher oxygen content (0.75 wt-%), the amount of NiO crystals increases as Ni content increases. (Forsén, 1985.) A small fraction of the nickel in the anodes can also form nickel ferrite ($NiFe_2O_4$) or a Cu−Ni−Fe oxide phase. Some of the nickel containing elements in the anodes are presented in figure 5. (Chen & Dutrizac, 1990a.)

In the presence of antimony in nickel-rich anodes, kupferglimmer (Cu-Ni-Sb oxide) forms. According to Chen and Dutrizac (1989b), the nickel content has to be over 0.3 % and the antimony content higher than 200 ppm in order for kupferglimmer to form. In their experiments, synthetic kupferglimmer had the formula $Cu_3Ni_{2-x}SbO_{6-y}$, where x = 0.1-0.2. Kupferglimmer formed complex inclusions along the copper grain boundaries together

with $Cu_2Se$, Cu−Pb−As oxide, $Cu_2O$ and NiO (figure 6). (Chen & Dutrizac, 1989b.)

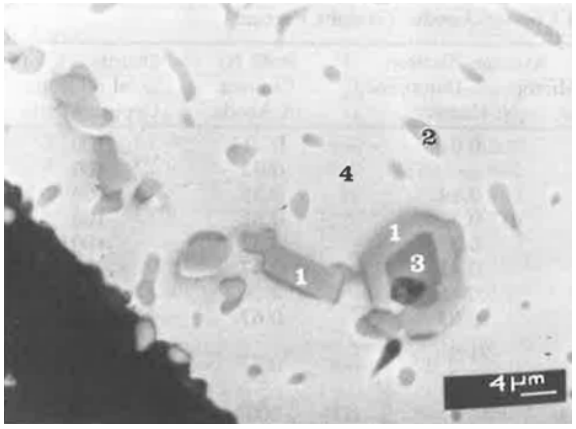


Figure 5: BSE image of a polished copper anode, showing a $NiFe_2O_4$ crystal with a NiO rim. 1: NiO 2: $Cu_2O$ 3: $NiFe_2O_4$ 4: copper matrix. (Chen & Dutrizac, 1990a.)

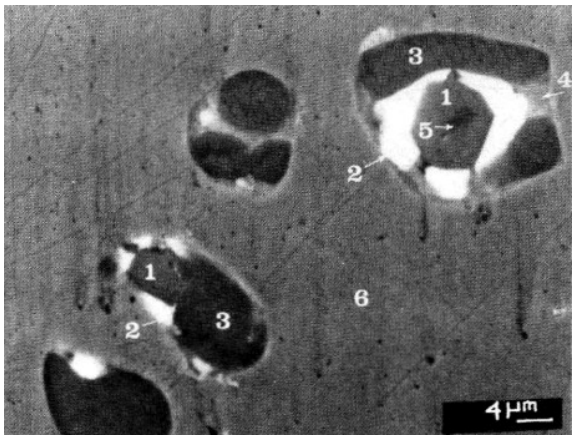


Figure 6: BSE image of a polished copper anode, showing the general morphology of kupferglimmer. 1: Kupferglimmer 2: Pb−As−Cu oxide 3: $Cu_2O$ 4: $Cu_2Se$ 5: NiO 6: copper matrix. (Chen & Dutrizac, 1990a.)

### 2.2.3 Arsenic, antimony, bismuth and lead

The complex oxides in the copper anodes are important carriers of arsenic, antimony, bismuth and lead. The arsenic, antimony, bismuth and lead containing complex oxides are Cu−Pb−As, Cu−Pb−Sb, Cu−Pb−Bi, Cu−Bi−As, Cu−Pb−As−Sb, Cu−Pb−As−Sb−Bi and Cu−Pb oxides. These species often occur in complex inclusions together with $Cu_2O$, $Cu_2$(Se,Te) and kupferglimmer. (Chen & Dutrizac, 1990b.)

According to Chen & Dutrizac (1990b), arsenic and lead can also be present in the cop-

per matrix at relatively low concentrations. In the PIXE analysis performed by Chen and Dutrizac (1993) on anodes with arsenic concentrations ranging from 600 ppm to 1900 ppm, it seemed that around 38 % of the total arsenic content was in solid solution with copper. In the same experiments, around 23 % of the total antimony content was also found in solid solution with copper, the antimony concentrations ranging between 100 and 1300 ppm. In their research from 1991, around 60 % of the total arsenic content was found in solid solution with copper in anodes containing 1200 ppm of arsenic.

### 2.2.4 Silver, selenium and tellurium

According to Chen and Dutrizac (1989a), the main silver carrier in the copper anodes is the copper matrix. In the anodes that they examined, over 95 % of the silver was found in solid solution with copper. In silver-rich anodes, silver also occurs in ($Cu_2$(Se,Te)) inclusions and on rare occasions in the complex Cu−Pb−As−Sb−Bi oxide phase. (Chen & Dutrizac, 1989a.)

In the copper anodes, selenium is mainly present in the $Cu_2$(Se,Te) phase. The $Cu_2$(Se,Te) particles typically appear together with $Cu_2O$ and other oxides (figure 7). The $Cu_2$(Se,Te) $-Cu_2O$ inclusions usually occur at the copper grain boundaries. (Chen & Dutrizac, 1990b.) Figure 7 presents multiple $Cu_2O$-$Cu_2$(Se,Te) inclusions around a copper crystal. In the PIXE analysis that Chen and Dutrizac (1993) performed, it was found that selenium and tellurium also occur in solid solution with copper. Based on the analysis it seemed that the copper became "saturated" with selenium at low total selenium concentrations. The same "saturation" effect was observed with tellurium.

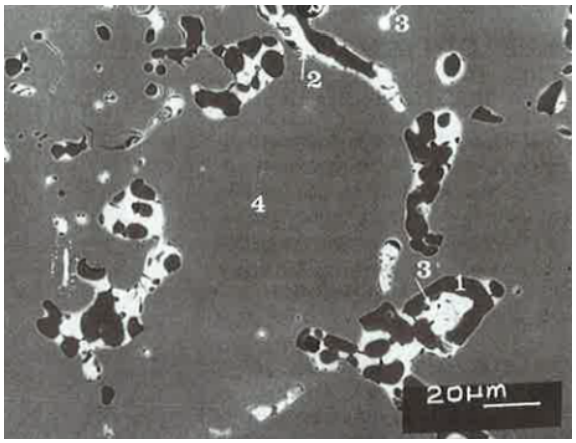


Figure 7: BSE image of a polished copper anode, showing multiple $Cu_2O$-$Cu_2$(Se,Te) inclusions around a copper crystal. 1: $Cu_2O$ 2: $Cu_2$(Se,Te) oxide 3: silver alloy 4: copper crystals. (Chen & Dutrizac, 1993.)

## 2.3 Anode slime formation

The impurities in copper anodes dictate to a large degree the composition of the anode slimes. As the copper anode dissolves, its impurities are continuously released from the copper matrix and the grain boundaries. (Cheng & Hiskey, 1996.) The deportment of different anode impurities to the anode slimes and to the electrolyte is presented in table 5. The released impurities can stay unchanged or go through chemical or electrochemical reactions (Cheng & Hiskey, 1996). The species that can be present in anode slimes, according to Cheng and Hiskey (1996), are presented in table 6.

Table 5: The deportment of anode impurity elements, adapted from (Larouche, 2001; Schlesinger et al. 2011).

| Element | Deportment to slimes, % | Deportment to electrolyte, % |
|---|---|---|
| Cu | < 0.2 | > 99.8 |
| Ag | > 99 | < 1 |
| Se | 98 | 2 |
| Te | 98 | 2 |
| Pb | 98 | 2 |
| Bi[a] | 60 | 40 |
| Sb[b] | 60 | 40 |
| As[c] | 25 | 75 |
| Ni* | 1 | 99 |

a: With 0.1 % Pb in anode.
b: With 0.1 % As, Bi, Pb and Sb (each) in anode.
c: With 0.1 % As in anode.
*: The deportment of nickel depends largely on the nickel content of the anode.

Table 6: The possible species in anode slimes, adapted from (Cheng & Hiskey, 1996).

| Group VA: **As Sb Bi** | Group VIA: **O S Se Te** | Group IB: **Cu Ag Au** | Group IVB: **Sn Pb** | Other Elements: **Fe Ni Zn** |
|---|---|---|---|---|
| $As_2O_3$ | Cu° Ag° Se° Au° | | $SnO_2$ | $Fe_2O_3$ |
| $Sb_2O_3$ | $Cu_2Se$ $Ag_2Se$ $Cu_2S$ | | $Sn(OH)_2 \cdot SO_4$ | $Fe_3O_4$ |
| $Bi_2O_3$ | CuAgSe $(Ag,Cu)_2Se$ | | $PbSO_4$ | NiO |
| $SbAsO_4$ | AgTe $(Ag,Au)Te_2$ $Cu_2(Se,Te)$ | | $xPbO \cdot As_2O_5$ | ZnO |
| $BiAsO_4$ | CuO $Cu_2O$ $Cu_2SO_4 \cdot 5\,H_2O$ | | $yPbO \cdot Sb_2O_5$ | $CuFe_2O_4$ $NiFe_2O_4$ |
| | $Cu_3(SbO_4)_2$ $Cu_3(AsO_4)_2$ | | $Pb(Sb,As)O_4$ | $3\,Cu_2O \cdot 4\,NiO \cdot Sb_2O_5$ |
| | $CuSeO_3 \cdot 2\,H_2O$ $SiO_2$ | | | $(Cu,Ni)SO_4 \cdot 5\,H_2O$ |

### 2.3.1 Anode slime types

The anode slimes can either adhere to the anode surface, fall to the bottom of the refining cell (Davenport et al. 2002) or form floating slimes in the electrolyte (Moats & Hiskey, 2010). Wang et al. (2011) classify the anode slimes as presented in figure 8. Primitive and secondary slimes are classified according to their formation mechanisms. Primitive slimes consist of the species that already exist in the anode and which remain unchanged through electrorefining. These species are typically noble metals, sulphides and selenides. The secondary slimes, on the other hand, consist of compounds that form after the actual dissolution. These compounds are typically arsenato antimonates, $PbSO_4$ or AgCl. (Wang et al. 2011.)

The secondary slimes can be categorized further into first reaction and second reaction slimes. The first reaction slimes are species that form directly in the electrolyte after the dissolution. The second reaction slimes are typically formed in an oxidation reaction with the $O_2$ dissolved in the electrolyte. Typical second reaction slime species are precipitates of arsenato antimonates, antimonates and metal high valence oxides. The second reaction slimes can either form floating or normal slimes.

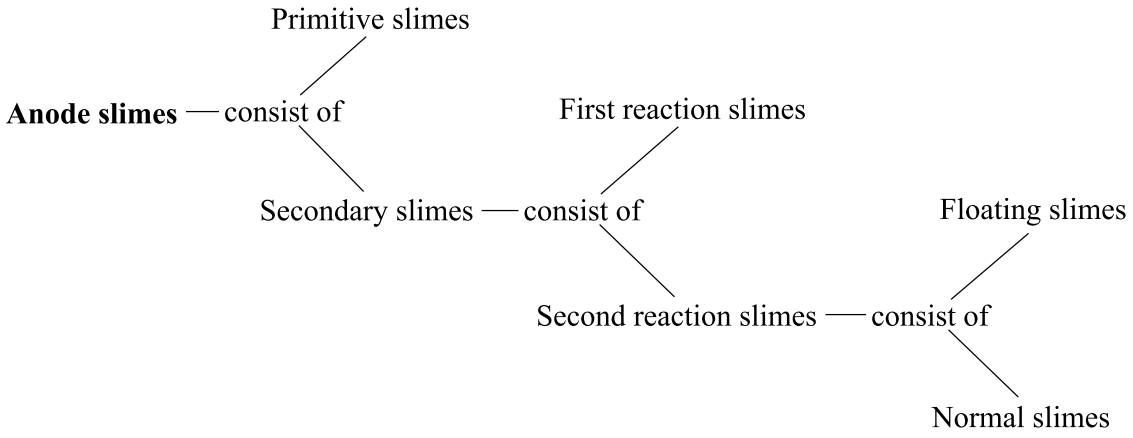


Figure 8: Anode slime types, adapted from (Wang et al. 2011).

### 2.3.2 Anode passivation

As mentioned already in the introduction of the thesis, the formation of adherent anode slimes can inhibit the anode dissolution. If the dissolution is completely inhibited, the anode passivates. (Moats & Hiskey, 2010.) The formation of adherent anode slimes and the phenomenon of anode passivation are therefore closely linked and can be studied with

the help of chronopotentiograms. In chronopotentiometric measurements the potential of the anode is measured over time in constant current conditions.

The chronopotentiometric tests performed on commercial copper anodes by Cheng and Hiskey (1996) show four distinctive areas, presented in figure 9. Region I is the region of active dissolution, II the region of prepassivation, III the area of passivation onset and IV is the actual passivation region. On the passivation area, anode slime consists mainly of $Cu_2O$. (Cheng & Hiskey, 1996.) A similar kind of chronopotentiogram (figure 10) was presented by Moats and Hiskey (2010), which shows the same four regions as figure 9 does.

In terms of adherent anode slime formation and anode passivation, the regions of interest are regions I and II, preceeding the passivation. As Moats and Hiskey (2010) explain it, in the region I, the application of current causes anode dissolution to begin. The potential is quite stable, yet slightly increasing. The increase in potential in the region I is due to the anode surface becoming partially covered with adherent anode slimes. The adherent anode slimes restrict the anode dissolution to their pores and decrease the active surface area. The decrease in the active surface area causes an increase in current density on the remaining surface area which, in turn, increases the potential. (Moats & Hiskey, 2010.)

In the region II, potential oscillations begin to occur. These oscillations can be explained by $CuSO_4 \cdot 5\,H_2O$ which precipitates and dissolves on the anode surface, in the pores of the adherent anode slimes. (Moats & Hiskey, 2010.) In the studies of Moats and Hiskey (2010), the potential oscillations started when the calculated surface coverage was between 85 % and 95 %. The increase of potential in the oscillations of region II would also indicate an increase of the adherent anode slimes, $CuSO_4$ and $Cu_2O$ on the anode surface. The oscillations become more uniform. This is caused by $CuSO_4$ which forms as copper dissolves in the pores of the adherent anode slimes. At the interface of the anode surface and $CuSO_4$, $Cu_2O$ starts to form. Once the anode passivates, the $CuSO_4$ dissolves and exposes the $Cu_2O$. Also the $Cu_2O$ dissolves over time and and exposes some anode surface. The anode dissolution will then start again and the cycles of precipitation and dissolution will continue with increasing potentials until the potential is high enough to stabilize the $Cu_2O$. (Moats & Hiskey, 2010.)

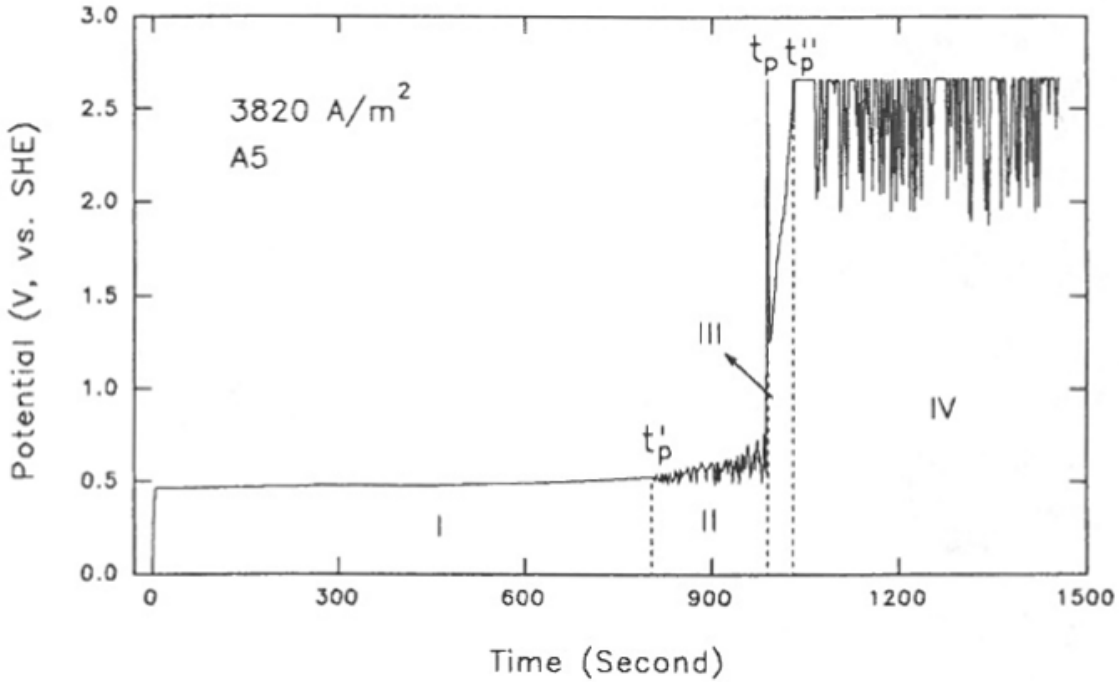


Figure 9: Chronopotentiogram (Cheng & Hiskey, 1996)

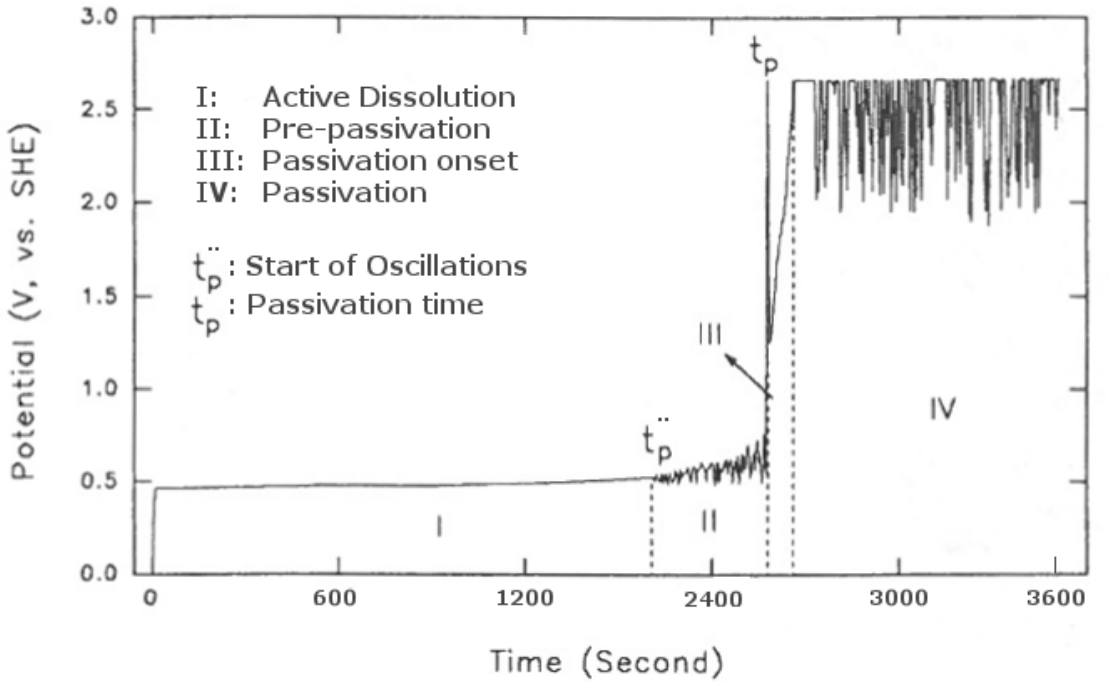


Figure 10: Chronopotentiogram (Moats & Hiskey, 2010)

## 2.4 Adherent anode slime composition and morphology

In the following subchapters, some of the anode slime species will be discussed in more detail. Table 7 summarizes the dominant and minor phases of the impurity elements of interest in anode slimes.

Table 7: The anode slime species, adapted from (Chen & Dutrizac, 1990b).

| Element | Dominant phases | Minor phases |
|---|---|---|
| Cu | | $CuSO_4 \cdot 5\,H_2O$<br>$Cu_2O$<br>$(Cu,Ni)SO_4 \cdot 5\,H_2O$<br>Complex oxides |
| O | $CuSO_4 \cdot 5\,H_2O$<br>Complex oxides | NiO |
| Ag | Ag-Cu selenides<br>Metallic Ag | Complex oxides<br>Cu-Ag sulfate |
| Ni | | $NiSO_4 \cdot nH_2O$<br>$(Cu,Ni)SO_4 \cdot 5\,H_2O$<br>Complex oxides<br>NiO<br>$NiFe_2O_4$<br>Cu−Ni−Fe oxide<br>Kupferglimmer |
| As | Complex oxides | $SbAsO_4$<br>$BiAsO_4$ |
| Sb | Complex oxides | $SbAsO_4$ |
| Bi | Complex oxides | $BiAsO_4$ |
| Pb | $PbSO_4$ | Complex oxides |
| Se | Ag-Cu selenides | |
| Te | Selenide-solid solution | Complex oxides |

### 2.4.1 Oxygen

According to Chen and Dutrizac (1990b), the important oxygen bearing species in the anodes, $Cu_2O$, is in fact rare in the anode slimes. The reason why $Cu_2O$ is rare in the anode slimes is its rapid dissolution once exposed to the electrolyte.

In the anode slimes, oxygen bearing species are $CuSO_4 \cdot 5\,H_2O$ and different oxides, such as the complex oxides, NiO and kupferglimmer (Chen & Dutrizac, 1990b). From table 6 it can be seen that most of the anode slime species contain, in fact, oxygen. According to Cheng and Hiskey (1996), oxygen appears to have a great influence on the anode slime chemistry and morphology.

### 2.4.2 Nickel

The majority of the nickel found in solid solution in the copper matrix dissolves in the electrorefining process. However, a small amount of the nickel can reprecipitate as $NiSO_4 \cdot nH_2O$, $(Cu,Ni)SO_4 \cdot 5\,H_2O$ or as complex oxides. In the anodes that have a high nickel concentration, possible nickel bearing species in the anode slimes are also NiO, kupferglimmer, $NiFe_2O_4$ and $Cu-Ni-Fe$ oxide. (Chen & Dutrizac, 1990b.) As table 5 indicates, only about 1 % of the total nickel content deports to anode slimes. Table 8 summarizes the different nickel bearing species in the anodes and the anode slimes.

Table 8: The nickel containing species in the anodes and the anode slimes, from (Chen & Dutrizac, 1990a)

| **Nickel in anodes** | | **Nickel in anode slimes** |
|---|---|---|
| **< 0,3 %** | **> 0,3 %** | |
| Solid solution | Solid solution | $NiSO_4 \cdot nH_2O$<br>$(Cu,Ni)SO_4 \cdot 5\,H_2O$<br>complex oxidate phase |
| | NiO<br>$NiFe_2O_4$<br>$Cu-Ni-Fe$ oxide<br>Kupferglimmer | NiO<br>$NiFe_2O_4$<br>$Cu-Ni-Fe$ oxide<br>Kupferglimmer |

### 2.4.3 Arsenic, antimony, bismuth and lead

Arsenic, antimony and bismuth occur in complex oxides in the anode slimes. The precipitation of $SbAsO_4$ and $BiAsO_4$ from the electrolyte into the anode slimes is also possible. (Chen & Dutrizac, 1990b.)

As the lead in the complex oxides and in the copper matrix dissolves, it reacts with the $H_2SO_4$ of the electrolyte and forms lead sulfate ($PbSO_4$) (Chen & Dutrizac, 1990b). As

the formation of $PbSO_4$ happens quickly after dissolution, $PbSO_4$ precipitates on the surface of the anode (Moats et al. 2012). $PbSO_4$ can occur together with selenides or as euhedral crystals or crystal clusters in the anode slimes (Chen & Dutrizac, 1990b).

### 2.4.4 Silver, selenium and tellurium

What comes to silver, selenides are an important silver carrier. There can also be metallic silver present in the anode slimes. The amount of metallic silver depends on the Ag/Se molar ratio of the anode. Cu-Ag sulfate can also be present. (Chen & Dutrizac, 1990b.) Figure 11 presents silver crystallites on the anode slime surface. It is thought that during the copper anode dissolution, the dissolved silver reacts with the $Cu_2Se$ inclusions and forms various $Ag-Cu$ selenides (Chen & Dutrizac, 1990b). Figure 12 shows a typical selenide ring. The majority of the tellurium in anode slimes is in solid solution with the selenides. A small amount of tellurium can also contribute to the complex oxidate phase.

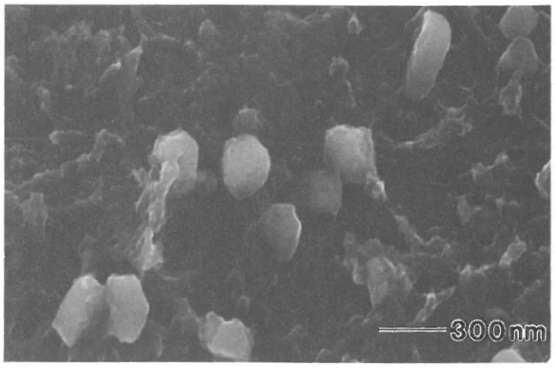


Figure 11: A FESEM micrograph presenting silver crystallites (Cheng & Hiskey, 1996).

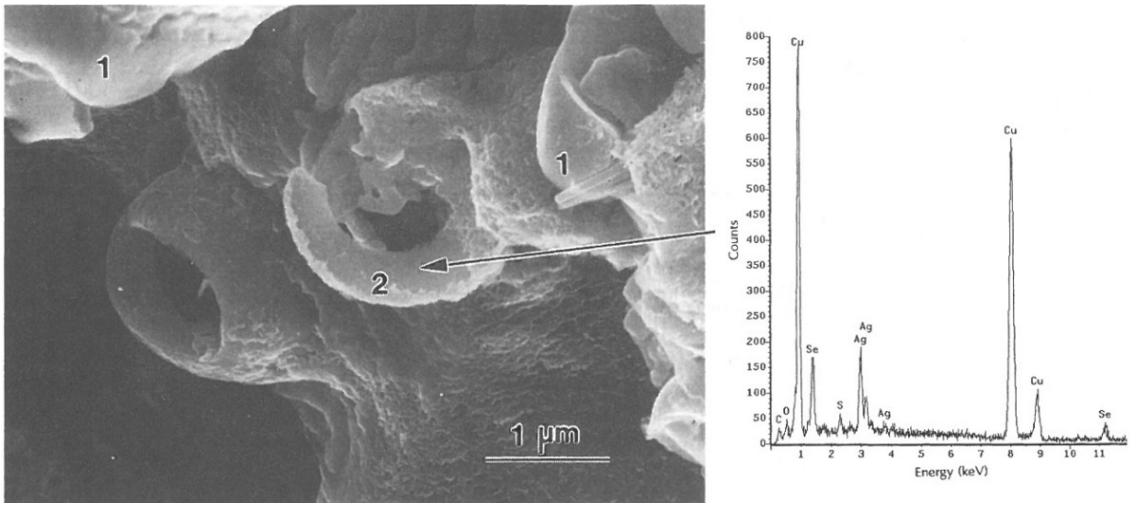


Figure 12: A FESEM micrograph presenting a selenide ring (Cheng & Hiskey, 1996).

## 2.5 Factors affecting anode slimes

In the following subchapters the effects of different factors on the formation of adherent anode slimes are discussed. The factors discussed include different anode impurities and electrolysis conditions, namely electrolyte properties and current density. In terms of the anode impurities, the anode slime properties of interest are the amount of anode slimes produced and the adherence of the slimes. A summary of the effects of the anode impurities on anode slimes are presented in table 9. All in all, not much data was found in literature of the species causing increased adherence of the anode slimes.

Table 9: The effect of different impurity elements on the amount and adhesion of anode slimes, adapted from (Gu et al. 1995; Krusmark et al. 1995; Moats & Hiskey, 2010; Möller et al. 2010; Moats et al. 2012). "+" stands for an increase and "-" for a decrease.

| Impurity element | Amount | Adhesion |
|---|---|---|
| O | + | |
| Ag | + | |
| Ni | + | |
| As | - | - |
| Pb | + | |
| As/(Sb+Bi) < 2 | | + |
| Se | + | |
| Te | + | |

### 2.5.1 Oxygen and nickel

Oxygen increases the amount of anode slimes produced unless paired with arsenic or high current densities (Möller et al. 2010). Demaerel (1987) found that the increase of oxygen content in the anode decreases the settling rate of the forming anode slime. The increase of oxygen content also decreased the amount of arsenic reporting to the slimes (Demaerel, 1987). Oxygen also increases the anode dissolution rate. It also seems that oxygen increases the distribution of antimony to the anode slimes. (Möller et al. 2010.)

NiO and kupferglimmer do not dissolve in the electrolyte. Therefore, these compounds will contribute to the formation of an anode slime. In other words, if the concentration of these species in the anode is increased, also the amount of anode slimes is increased. (Moats & Hiskey, 2010.)

### 2.5.2 Arsenic, antimony, bismuth and lead

Already in 1987, Demaerel observed that in fixed impurity level anodes the increase in arsenic content decreased the amount of adherent anode slimes. Also Krusmark et al. (1995) observed that anodes with low arsenic content produced slimes that were more adherent to anode scrap during washing. Krusmark et al. (1995) also observed that a low As/(Sb+Bi) ratio leads to more adherent anode slimes. also observed that Möller et al. (2010) report that arsenic lowers the amount of anode slimes produced.

As already discussed earlier, the dissolved lead forms $PbSO_4$ on the anode surface (Moats et al. 2012). Therefore, the higher the lead content of the anode, the more adherent anode slimes are produced.

### 2.5.3 Silver, selenium and tellurium

According to Gu et al. (1995), silver increases the amount of suspended anode slimes. According to Moats and Hiskey (2010), both selenium and tellurium are common slime forming elements. $Cu_2Se$ and CuTe, the species in which selenium and tellurium are mainly present in the anodes, dissolve slowly into the electrolyte and form therefore a part of the anode slimes. Increasing the amount of selenium and tellurium in the anodes would result in the increase of anode slimes. (Moats & Hiskey, 2010.)

### 2.5.4 Electrolyte properties and current density

As described in subchapter 2.3.2 Anode passivation, Moats and Hiskey (2010) explain anode passivation with the formation of non-conducting or weakly conducting films on the anode surface, such as adherent anode slimes, $CuSO_4 \cdot 5\,H_2O$ and $Cu_2O$. When the anode surface is completely covered with these films, the anode passivates. (Moats & Hiskey, 2010).

In their earlier study (2007), Moats and Hiskey stated that since $CuSO_4 \cdot 5\,H_2O$ forms on the anode surface via precipitation, the electrolyte components that affect the solubility of $CuSO_4$ also affect anode passivation. Increasing copper and acid concentrations in the electrolyte would therefore lead to faster precipitation of $CuSO_4 \cdot 5\,H_2O$ on the anode surface (Moats & Hiskey, 2007).

Electrolyte pH and cuprous ion ($Cu^+$) concentration can affect the formation of $Cu_2O$. Therefore, the electrolyte parameters that affect the pH and the cuprous ion concentration can also affect anode passivation. Adsorbed organic molecules from electrolyte additives can form non-conductive films on the anode surface, also. (Moats & Hiskey, 2007).

According to Moats and Hiskey (2010), the electrorefining conditions do not really affect the amount of slimes formers. However, applied current affects the formation rate of the slimes (Moats & Hiskey, 2010). Excessive current densities might lead to anode passivation due to the production of $Cu^{2+}$ ions faster than they can diffuse and convect away from the anode surface (Schlesinger et al. 2011).

# 3 Experimental methods and materials

Figure 13 presents the goals of the thesis and the methods used as a chart. The main goal of the thesis was to produce information of the adherent anode slimes for the SIMP programme. This producing of information included characterization of the anode and adherent anode slime samples with the help of different analyses, which were performed in the order of figure 14. More specifically, a reason for the varying adherent anode slime amount and adherence was tried to be found. For Boliden Pori electrorefinery and for Outotec Research Center, Pori, the collecting of an anode slime "library" and the establishing of a handling process for the anode slime samples were important goals, also.

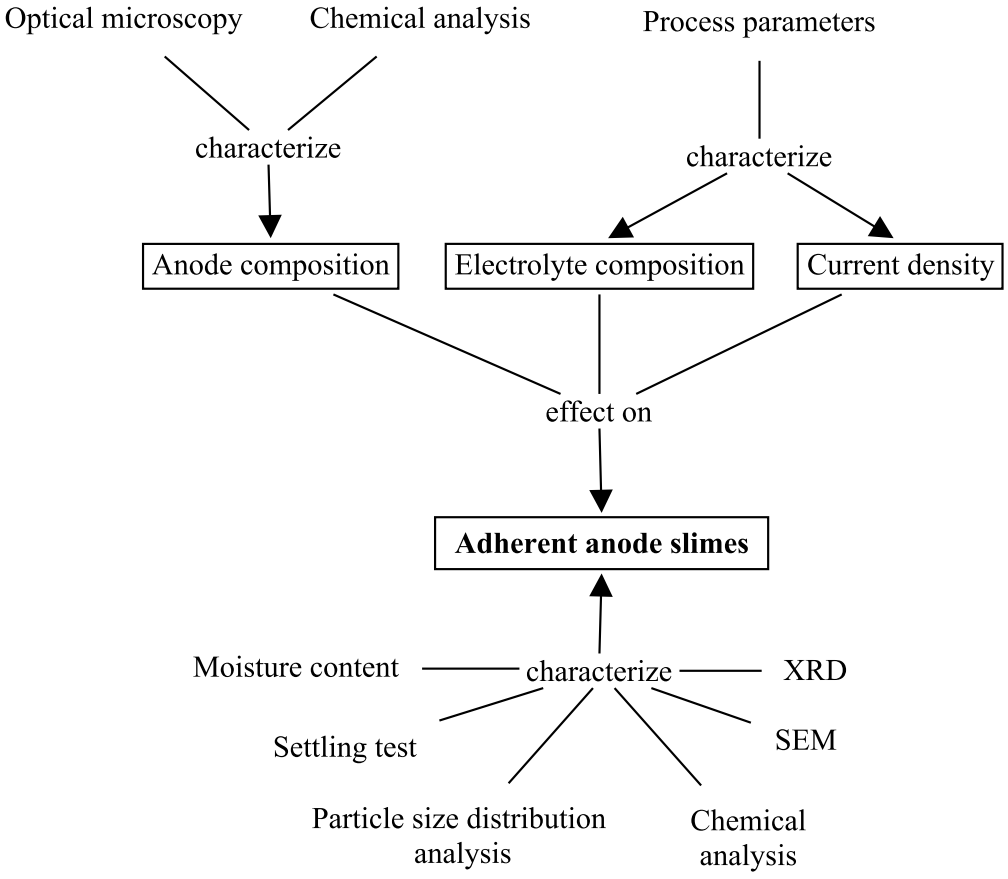


Figure 13: A chart presentation of the goals and methods of adherent anode slime characterization.

As figure 13 implies, the effect of anode and electrolyte composition and current density on the adherent anode slimes were also studied. Anode composition was examined with the help of optical microscopy and chemical analysis. Information concerning the elec-

trolyte composition and the current density were obtained from the process parameters of Boliden Pori electrorefinery.

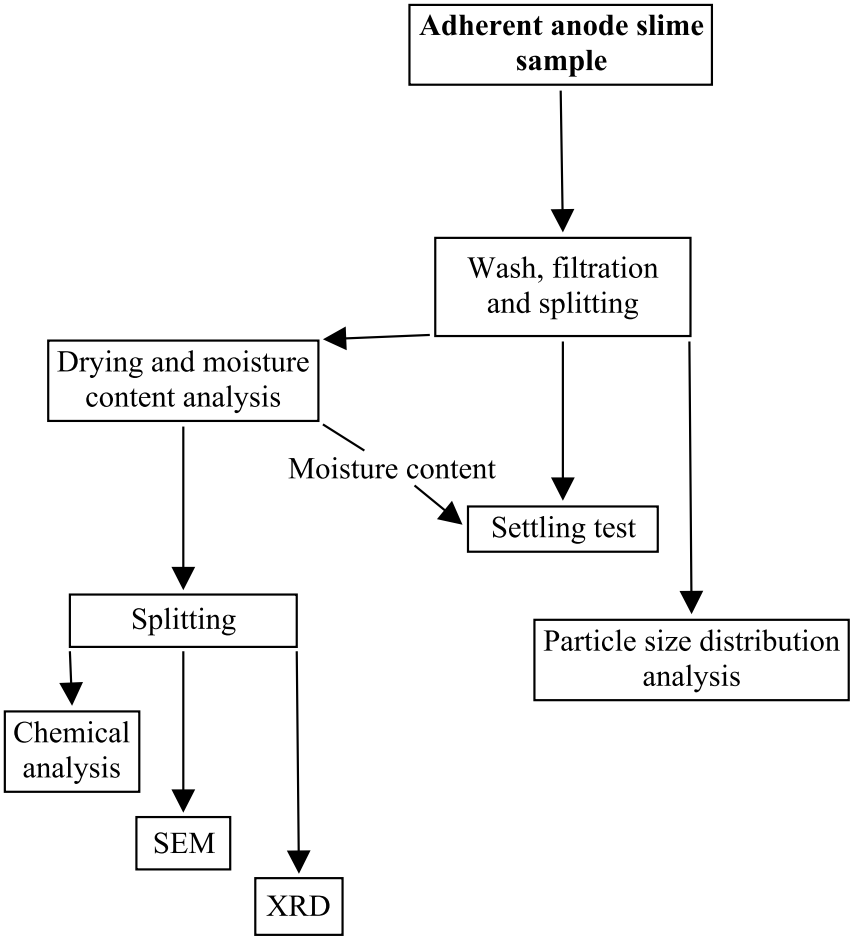


Figure 14: The order of the analyses

## 3.1 Sampling

The adherent anode slime and anode lug samples were taken at Boliden Pori electrorefinery, during 31.3.-19.4.2014. In total, 31 anode lug and adherent anode slime samples were obtained.

The adherent anode slime samples were collected in the end of the electrolysis cycle, at the washing station. The samples were collected by different people which resulted in varying sampling techniques. Due to varying sampling techniques, some of the adherent anode slime samples were taken from both sides of the anode and some only from one side. Also the moisture content and the amount of adherent anode slime samples varied.

Figures 15 and 16 present the extremes in sample moisture content and sample amount variation, respectively, before the sample preparation.

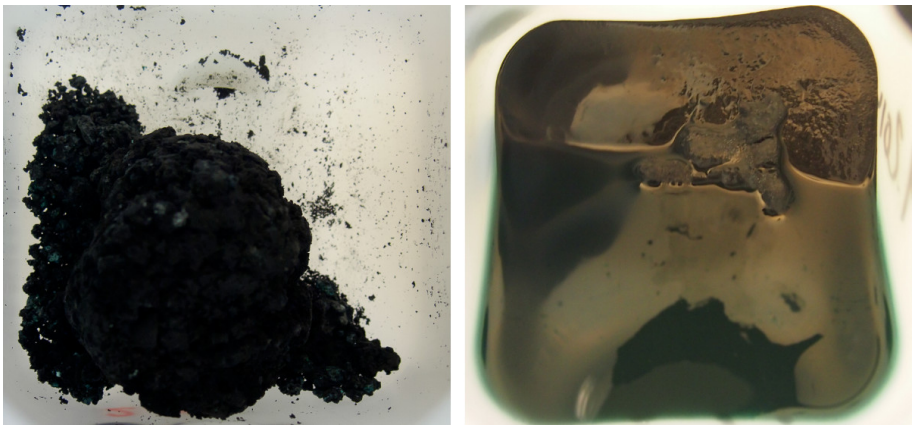

Figure 15: The extremes of sample moisture content variation, before sample preparation. © CORR

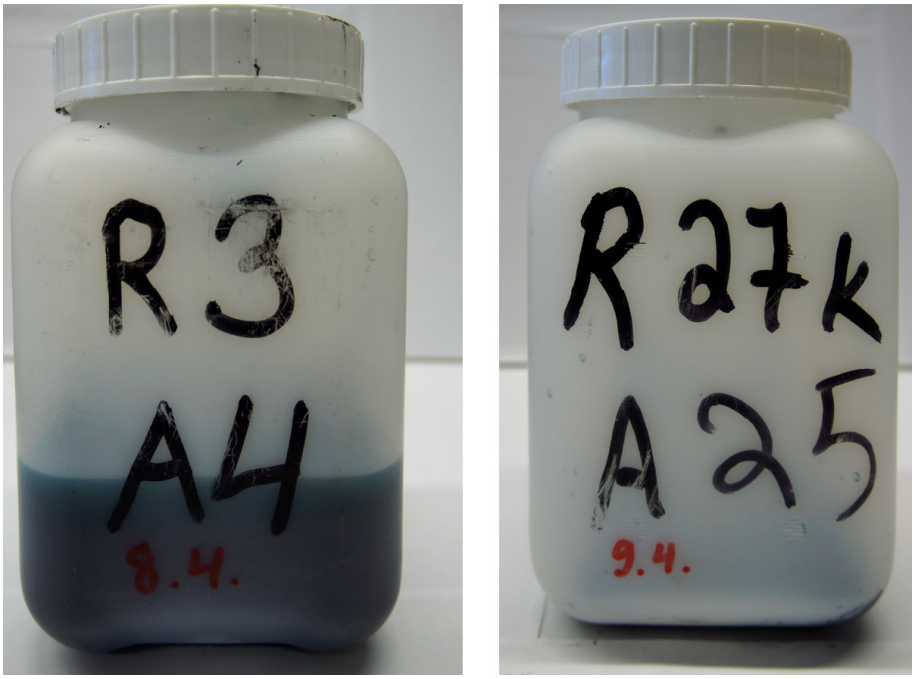


Figure 16: The largest and the smallest adherent anode slime sample. © CORR

## 3.2 Sample preparation

Before the analyses, the samples were washed and filtered in order to remove most of the electrolyte from them. Before the washing, the sample containers were weighed and

photographed. In total, eight of the adherent anode slime samples had dried out and had to be leached into water before the actual washing. The amount of water used in the leaching of the dried samples was 200 ml or 300 ml, depending on the amount of the sample.

The slimes were washed and filtered in a 15 cm diameter Bühner funnel attached to a 1 liter Erlenmyer flask. In the filtering, a filtering paper of type Munktell 100053, grade 00M, was used. The filtering paper sheets were cut to circles, their diameters ranging from 17 cm to 19 cm, depending on the amount of the sample. This was done to create 1 cm to 2 cm borders which prevented the loss of the slime sample during rinsing. The filtering papers were weighed both dry and wet, so that it would be possible to determine the sample residue amount in the filtering paper, later on.

The amount of water used in the washing varied between 1500 ml and 3500 ml of water, depending on the amount of the sample. The slime samples were washed until the color of the rinsing water was close to that of distilled water. On average, the washing took from 20 to 30 minutes and with the largest samples, from 40 to 60 minutes.

The washed and filtered slime cake was photographed and split into four sections. Before the splitting, the slime cake was weighed in order to obtain fractions of close to equal masses. The slime cake masses varied between 384.10 g (sample 15. R3 A4) and 24.70 g (sample 16. R27k A25). All of the analyses could be performed on the samples that had a slime cake mass larger than 50 g. Three of the 31 adherent anode slime samples (16. R27k A25, 24. R27s A7 and 31. R25 A29) had a smaller slime cake mass. In order to ensure the representativeness of the samples, the splitting of the slime cakes was done as figure 17 indicates. One of the fractions was dried with a drier and one was analysed with a particle size analyser. The two remaining sections were used in settling tests. On average, 5.43 g of each adherent anode slime sample was lost during sample preparation.

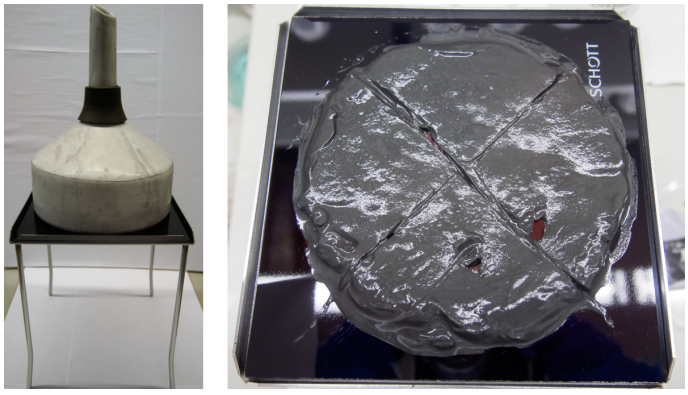


Figure 17: On the left, the flipping of the slime cake and on the right, the slime cake split. © CORR

## 3.3 Drying

The adherent anode slime samples had to be dried in order to obtain their moisture contents. The information of the moisture contents of the samples was needed for the settling tests. Drying was also required as a preparation step for the chemical, XRD and SEM analyses.

The drying of the slime samples was performed with a Radwag dryer, type MA 60.3Y.WH, presented in figure 18. The sample was loaded onto an aluminium drying pan. Two filtering papers were used between the pan and the samples in order to prevent the pan from corroding. The filtering papers were dried for 10 minutes in 60 °C temperature before the actual sample was dried. This was done to ensure that the sample result would be as accurate as possible.

The drying temperature was 60 °C and the drying time 20 hours for each slime sample. The maximum amount of sample that could be dried with the drier was 60 g. The obtained moisture contents are presented in chapter 4.1 Moisture contents and settling.

In order to ensure the representativeness of the sample fractions undergoing chemical, XRD and SEM analyses, the dried adherent anode slime powder was split into 20 fractions with a powder sample splitting system, presented in figure 19. A separate spinning riffler (Microscal L/MSR) and a vibratory feeder (Fritch Laborette 24.002) were used. The obtained fractions were combined to create 3 fractions for the chemical, XRD and SEM analyses. The goal was to obtain 5 g of the sample for the chemical analysis, 2 g for the SEM analysis and around 1 g of the sample for the XRD analysis.

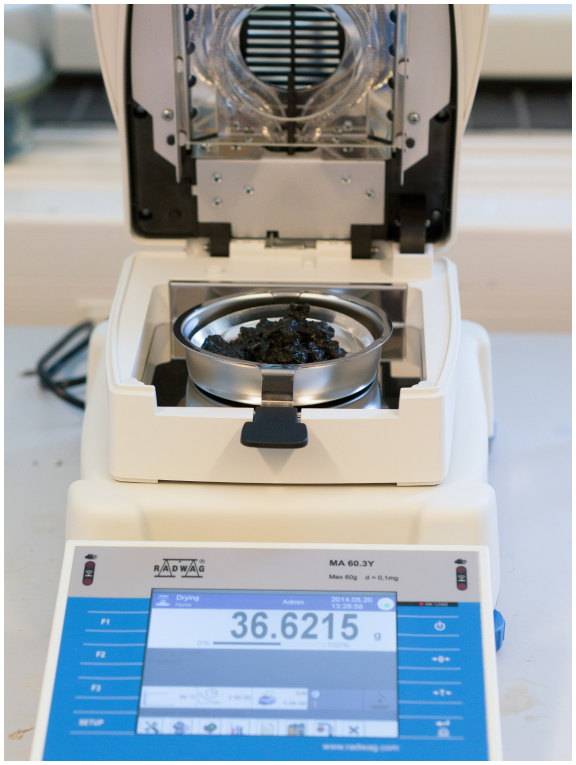


Figure 18: The Radwag dryer and an adherent anode slime sample on the drying pan. © CORR

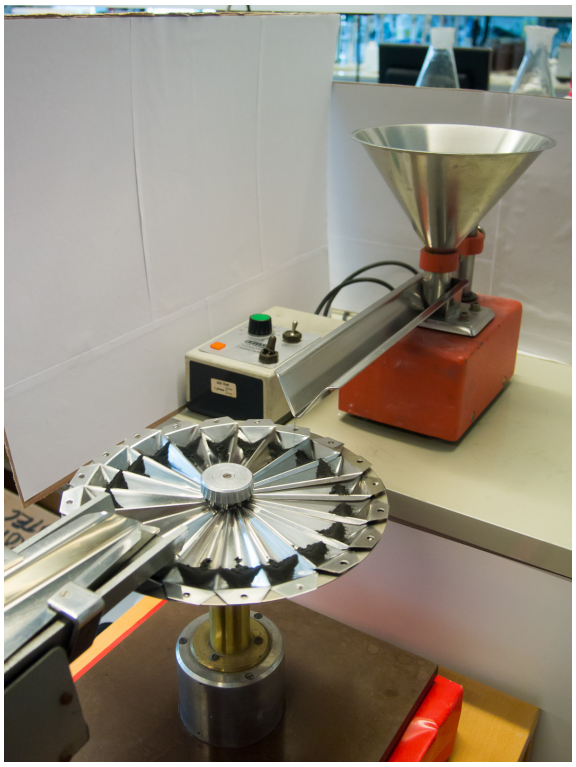

Figure 19: In the lower left corner, the spinning riffler and in the upper right corner, the vibratory feeder used in the splitting of the dried adherent anode slime samples. © CORR

## 3.4 Settling tests

In settling tests, the adherent anode slime sample is mixed into water to create a sludge. The sludge is placed into a measuring cylinder and with time, the sample particles fall to the bottom of the container, forming a sediment column and a clear supernatant. During settling tests, the height of the sediment column and the clarity of the supernatant will be observed and documented.

Settling tests provide information of the falling rate of the adherent anode slime particles. If the falling rate of the adherent anode slime particles is slow, the cathode might become contaminated. Combined with the moisture contents of the samples, settling tests might also provide information of the adherence of the anode slimes.

The settling tests were performed in a measuring cylinder of 250 ml, after the moisture contents of the samples were known. Based on the moisture content of the sample, a slime amount equivalent to 50 g/l was measured into a beaker. The slime was then mixed with water for five minutes and poured into the measuring cylinder. The adherent anode slime - water mixture was stirred for about one minute in the measuring cylinder, before starting the settling test.

In the settling tests, the height of the sediment column and the clarity of the supernatant were observed and documented during one hour. Pictures of the settling were taken once 1, 2, 5 and 60 minutes had passed.

## 3.5 Particle size distribution measurements

Particle size distribution measurements provide information of the particle size distribution of the adherent anode slime samples. Particle size distribution affects the settling rate of the slimes and there should therefore exist a connection between the settling rates and the particle size distributions of the samples.

The particle size measurements were performed with a Malvern Mastersizer 2000 particle size analyser. Each particle size measurement contained three repetitions. Distilled water was used as the dispersing agent.

In the measurements, the well mixed adherent anode slime was dosed in such a way that

the obscuration value of the analyser was between 8 % to 10 %. After the sample addition, the analyser ultrasound (value 13,5) was used for 5 minutes in order to break up possible agglomerates in the sample. After a 30 second wait, the measurement was started.

## 3.6 Chemical analysis

The chemical analysis provides information of the concentrations of the analysed elements in the anodes and the adherent anode slimes. Boliden Harjavalta provided the chemical analyses of the anodes. The dried adherent anode slime samples were sent to Labtium Oy for the chemical analysis.

The dried adherent anode slimes samples were sent to Labtium Oy in two lots. The first lot contained the first 13 samples and the second lot the samples from 14 to 31. With the samples of the first lot, 2 g of the sample was leached into aqua regia ($HNO_3$:HCl, 1:3), the end volume of the solution being 60 ml. The extraction was performed in 90 °C. After this, the concentrations of the elements were analysed with inductively coupled plasma mass spectrometry (ICP-MS) or with inductively coupled plasma atomic emission spectroscopy (ICP-OES).

In the laboratory of Boliden Harjavalta, the chemical compositions of some of the adherent anode slime samples were analyzed with x-ray fluorescence (XRF) analysis. When Labtium Oy's analysis results of the first lot were compared with the results of Boliden Harjavalta's XRF analysis, the concentration of silver was found to be too low in Labtium Oy's analysis. Because of this, Labtium Oy had to reanalyze the first sample lot with a modified sample preparation procedure.

In the modified sample preparation procedure, 0.05 g of the sample was leached into aqua regia, the end volume of the solution being 500 ml. The leaching was also performed in 90 °C. This analysis resulted in higher silver concentrations. The modified chemical analysis was used for the second sample lot, also.

## 3.7 X-ray diffraction (XRD)

XRD analysis can aid in the identification of different impurity species in the adherent anode slime samples. The XRD analysis consists of two phases: 1. the measurement

that provides the sample spectrum and 2. the identification of different species from the obtained sample spectrum. In the measurement phase, the x-ray source shoots and x-ray beam that is reflected from the sample onto the detector.

The dried adherent anode slime samples were analysed with a X'Pert PRO PANalytical PW3040/60 x-ray diffractometer. The slits that were used in the measurements are presented in table 10. For the samples, a 16 mm sample holder (figure 20) was used.

Table 10: The slits used in the XRD measurements.

| Slit | size |
|---|---|
| FDS | 0.5 |
| FASS | 1.0 |
| AS | 6.4 |
| Brass | 15 mm |

Figure 20: The XRD sample holder and a dried adherent anode slime sample. © CORR

The species that were analyzed from the XRD spectrums are presented in table 11 along with their reference numbers. The species of table 11 were chosen to be analyzed based on tables 6 and 7 and the chemical analysis of the adherent anode slimes, presented later in table 20.

Table 11: The species analyzed from the XRD spectrums with their reference numbers.

| Species | Reference number |
|---|---|
| $CuSO_4$ | 01-072-0090 |
| $Cu_2O$ | 01-077-0199 |
| Ag | 01-087-0717 |
| $PbSO_4$ | 01-089-7356 |
| $As_2O_3$ | 00-036-1490 |
| NiO | 00-044-1159 |
| Kupferglimmer | 00-043-0119 |
| $Ag_2Se$ | 00-024-1041 |
| AgTe | 00-016-0412 |

## 3.8 Scanning electron microscopy (SEM)

With the SEM analysis it is possible to examine the surface morphology and the different phases present in the adherent anode slime samples. The scanning electron microscope shoots an electron beam on the surface of the sample. When the electron beam hits the sample, it generates different signals that the corresponding detectors can interpret.

The adherent anode slime samples were prepared for the SEM as follows: a hydraulic press (Compac HP20 AA/AR) and a press cylinder were used to press 2 g of the dried adherent anode slime into a 11 mm diameter sample pellet. The pressure used was 5 tons.

The sample pellet was sealed into epoxy (Struers EpoFix Resin, 40200030) mixed with a hardener (Struers EpoFix Hardener, 40200087) and ground. In the grinding, grinding papers of grit 240, 400, 1200, 2000 and 4000 were used. After the grinding, the pellet micrograph was coated with carbon. In the carbon coating, a sputtering device (Leica EM SCD050) was used. After this, the scanning electron microscope (Tescan Mira 3 GMH) was used to take secondary electron (SE) images of the pellet micrographs.

## 3.9 Anode micrographs

From the anode lug samples, micrographs were made and examined with an optical microscope. This examination provides information of the microstructure of the anodes.

From the middle of the anode lug samples a piece was cut (figure 21). In order to prepare the micrograph, the piece was cast into epoxy (Struers EpoFix Resin, 40200030) mixed with a hardener (Struers EpoFix Hardener, 40200087), ground, polished and etched with ferric chloride solution. After the preparations, optical microscope Olympus PMG3 was used to take 5, 10 and 20 x magnifications of the micrographs.

In the casting, epoxy was used. In the grinding, grinding papers of grit 240, 400, 1200, 2000 and 4000 were used. After the grinding, the micrographs were polished with 3 $\mu$m and 1 $\mu$m polishing cloths together with diamond paste. The ferric chloride solution was prepared with 5 g of FeCl, 100 ml of $H_2O$ and 10 ml of HCl.

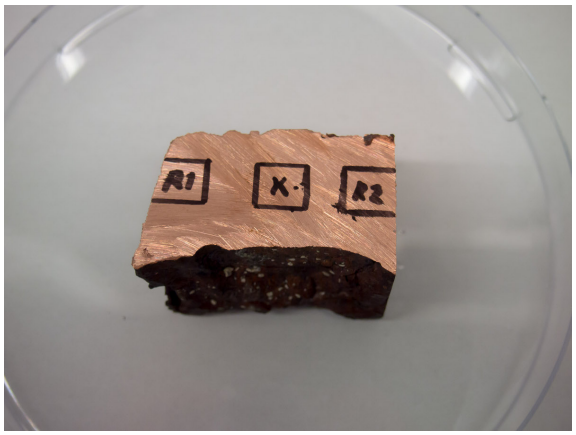


Figure 21: An anode lug sample with the micrograph piece still intact. The part used for the micrograph is presented with the letter "X". The area of the middle piece is approximately 1 $cm^2$. © CORR

# 4 Results and evaluation

In this section, the results of the performed analyses will be presented. All the sample names have the form "No. R A". The running number in the sample name relates to the age of the sample, number 1. being the first sample taken and number 31. the last one. Letter "R", followed by a number, corresponds to the anode group of the sample. Letter "A", followed by a number, corresponds to the electrolysis cell number from which the sample was taken.

The anodes were cast during 7.3.-28.3.2014. As mentioned already in chapter 3.1 Sampling, the anode and adherent anode slime samples were taken during 31.3.-19.4.2014. The majority of the analyses were performed on the samples between June and August 2014. On average, the samples were in storage for two months before the analyses. Since the sampling campaign was carried out during a relatively short period of time, no drastic differences were expected to occur in the samples.

## 4.1 Moisture contents and settling

The moisture contents of the adherent anode slime samples are presented in table 12, which shows that there is not much variation in the results. The average value of the sample moisture contents is 58.08 % and the standard deviation is 4.93 percentage points. Sample 23. R14 A9 has the highest moisture content (67.21 %) and sample 7. R17 A17 the lowest (45.77 %).

Table 13 presents the observed sediment column heights and the moments of time when a completely clear supernatant was observed in the settling tests. Results could be obtained for almost all of the samples, excluding samples 16. R27k A25, 24. R27s A7 and 31. R25 A29. Settling test results could not be obtained for these samples due to insufficient sample amounts. Also, the settling test result of sample 5. R13 A8 is unreliable due to the drying and insufficient dissolution of the sample before washing.

Table 14 presents a classification of the samples into groups of different settling rates, based on the sediment column heights of table 13. In table 14, the adherent anode slime samples have been divided into three groups. These three groups represent slow, intermediate and fast settling rates. Figure 22 presents graphs for one example sample from each group. Sample 9. R28s A34 is the example of the slow settling rate group, sample 11. R23

A16 of the intermediate group and sample 25. R16 A16 of the fast group.

As described in chapter 3.4 Settling tests, after 1, 2, 5 and 60 minutes photographs were taken of the settling of the adherent anode samples. The photographs taken during the settling test of the sample with a fast settling rate, 25. R16 A16, are presented in figure 23. Figure 24 presents the photographs taken during the settling test of the sample with a slow settling rate, 9. R28s A34.

Figure 22 shows clearly the differences between fast and slow settling rates. In the settling of sample 25. R16 A16, the sediment column almost reaches its end height after only one minute of settling. This is also evident in the photographs of figure 23. On the contrary, as can also be observed from the photographs of figure 24, in the settling of sample 9. R28s A34, the sediment column reaches its end height after three minutes of settling. The intermediate settling rate representative, sample 11. R23 A16, reaches the end sediment column height after two minutes of settling.

Interestingly, in the settling tests of both sample 9. R28s A34 and 25. R16 A16, the supernatant clarifies after 20 minutes. However, in the settling test of the example sample of the intermediate settling rate group, 11. R23 A16, the supernatant clarifies after 10 minutes of settling. The samples with a clear supernatant after 10 minutes of settling all fall into the intermediate and fast settling rate groups, as can be seen from table 14.

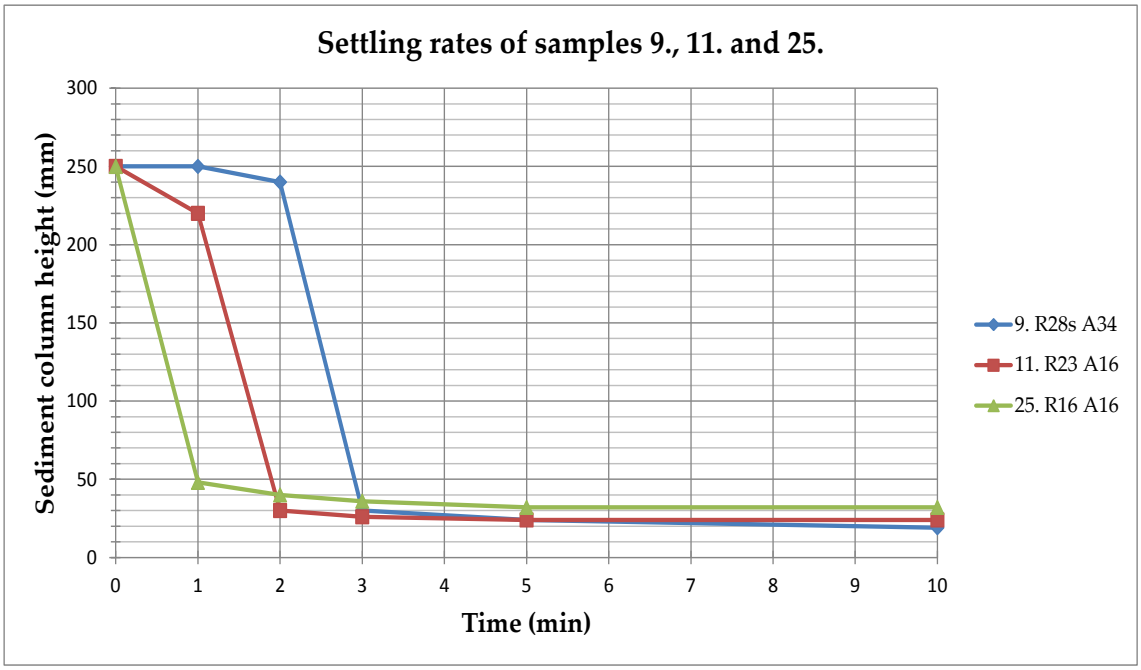


Figure 22: The sediment column heights of samples 9. R28s A34, 11. R23 A16 and 25. R16 A16, based on the information of table 13.

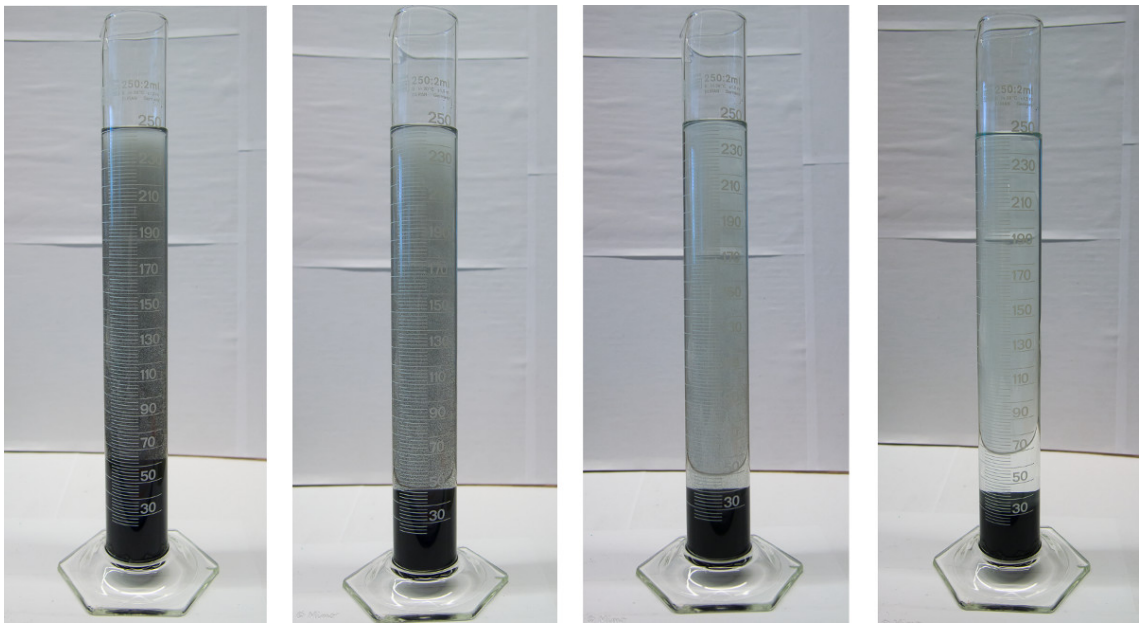

Figure 23: The settling of sample 25. R16 A16 after 1, 2, 5 and 60 minutes. © CORR

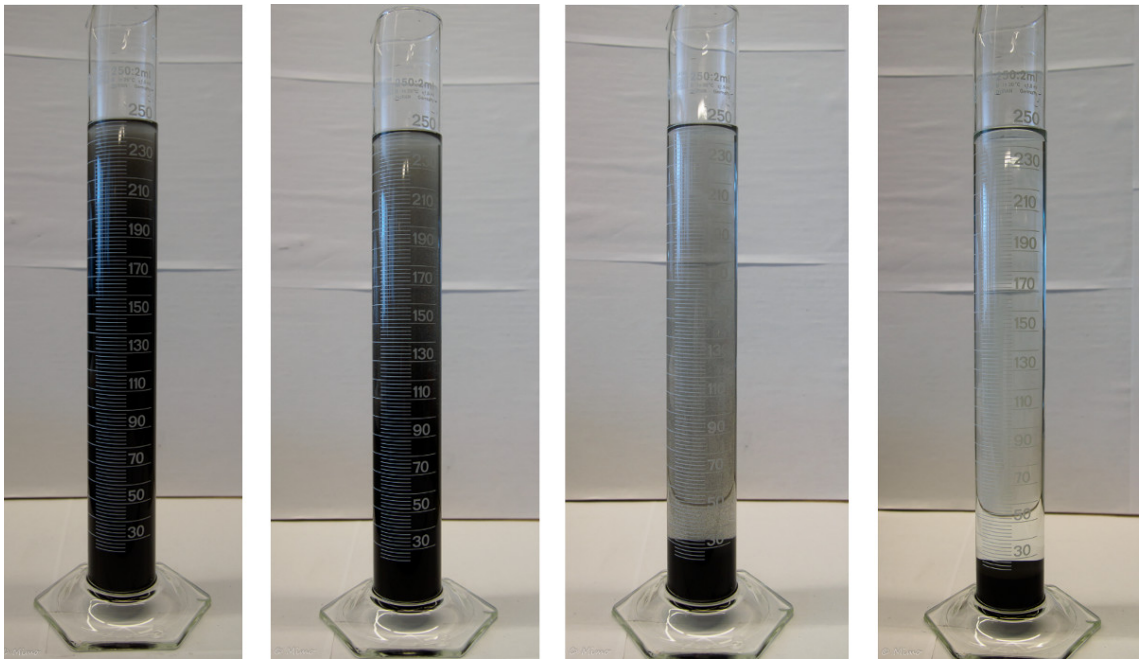

Figure 24: The settling of sample 9. R28s A34 after 1, 2, 5 and 60 minutes. © CORR

Table 12: The moisture contents of the adherent anode slime samples, in sample order.

| Sample | Moisture content (%) |
|---|---|
| 1. R24s A19 | 58.14 |
| 2. R11 A7 | 56.14 |
| 3. R24k A11 | 59.80 |
| 4. R20 A30 | 49.65 |
| 5. R13 A8 | 53.12 |
| 6. R8 A2 | 51.40 |
| 7. R17 A17 | 45.77 |
| 8. R9 A20 | 59.51 |
| 9. R28s A34 | 51.05 |
| 10. R7 A5 | 52.86 |
| 11. R23 A16 | 57.06 |
| 12. R18 A24 | 63.08 |
| 13. R2 A4 | 65.64 |
| 14. R15 A3 | 53.34 |
| 15. R3 A4 | 58.81 |
| 16. R27k A25 | 60.60 |
| 17. R10 A14 | 51.46 |
| 18. R5 A15 | 63.03 |
| 19. R19 A7 | 60.81 |
| 20. R4 A4 | 59.71 |
| 21. R26 A25 | 58.63 |
| 22. R21 A4 | 59.95 |
| 23. R14 A9 | 67.21 |
| 24. R27s A7 | 62.75 |
| 25. R16 A16 | 63.00 |
| 26. R28k A7 | 61.69 |
| 27. R12 A6 | 58.27 |
| 28. R22 A23 | 60.31 |
| 29. R1 A2 | 62.55 |
| 30. R6 A34 | 60.02 |
| 31. R25 A29 | 55.12 |

Table 13: The sediment column heights (mm) of the adherent anode slime samples at different times (min). The underlined column heights indicate the time of a completely clear supernatant (10 or 20 minutes). The sediment column heights of sample 5. R13 A8 have been included in the table in parentheses due to result unreliability.

| Sample | 0 | 1 | 2 | 3 | 5 | 10 | 20 | 30 | 45 | 60 | (min) |
|---|---|---|---|---|---|---|---|---|---|---|---|
| 1. R24s A19 | 250 | 240 | 30 | 28 | 26 | 26 | 26 | 26 | 26 | 26 | (mm) |
| 2. R11 A7 | 250 | 236 | 30 | 28 | 25 | 24 | 24 | 24 | 24 | 24 | (mm) |
| 3. R24k A11 | 250 | 240 | 47 | 33 | 30 | 28 | 28 | 28 | 28 | 28 | (mm) |
| 4. R20 A30 | 250 | 244 | 240 | 34 | 28 | 23 | 22 | 22 | 22 | 22 | (mm) |
| 5. R13 A8 | (250) | (250) | (210) | (110) | (22) | (20) | (20) | (20) | (20) | (20) | (mm) |
| 6. R8 A2 | 250 | 240 | 130 | 40 | 32 | 24 | 20 | 20 | 20 | 20 | (mm) |
| 7. R17 A17 | 250 | 220 | 26 | 21 | 18 | 18 | 18 | 18 | 18 | 18 | (mm) |
| 8. R9 A20 | 250 | 210 | 32 | 28 | 26 | 26 | 26 | 26 | 26 | 26 | (mm) |
| 9. R28s A34 | 250 | 250 | 240 | 30 | 24 | 19 | 18 | 18 | 18 | 18 | (mm) |
| 10. R7 A5 | 250 | 230 | 36 | 28 | 24 | 22 | 22 | 22 | 22 | 22 | (mm) |
| 11. R23 A16 | 250 | 220 | 30 | 26 | 24 | 24 | 24 | 24 | 24 | 24 | (mm) |
| 12. R18 A24 | 250 | 90 | 42 | 38 | 32 | 31 | 31 | 31 | 31 | 31 | (mm) |
| 13. R2 A4 | 250 | 75 | 56 | 40 | 36 | 34 | 34 | 34 | 34 | 34 | (mm) |
| 14. R15 A3 | 250 | 210 | 110 | 40 | 33 | 26 | 23 | 23 | 23 | 23 | (mm) |
| 15. R3 A4 | 250 | 70 | 36 | 32 | 29 | 28 | 28 | 28 | 28 | 28 | (mm) |
| 16. R27k A25 | | | | | | | | | | | |
| 17. R10 A14 | 250 | 200 | 110 | 22 | 20 | 18 | 18 | 18 | 18 | 18 | (mm) |
| 18. R5 A15 | 250 | 70 | 42 | 36 | 32 | 31 | 31 | 31 | 31 | 31 | (mm) |
| 19. R19 A7 | 250 | 110 | 48 | 38 | 32 | 30 | 30 | 31 | 30 | 30 | (mm) |
| 20. R4 A4 | 250 | 110 | 38 | 34 | 30 | 28 | 28 | 28 | 28 | 28 | (mm) |
| 21. R26 A25 | 250 | 50 | 34 | 30 | 27 | 27 | 27 | 27 | 27 | 27 | (mm) |
| 22. R21 A4 | 250 | 80 | 36 | 32 | 28 | 27 | 27 | 27 | 27 | 27 | (mm) |
| 23. R14 A9 | 250 | 48 | 37 | 34 | 33 | 33 | 33 | 33 | 33 | 33 | (mm) |
| 24. R27s A7 | | | | | | | | | | | |
| 25. R16 A16 | 250 | 48 | 40 | 36 | 32 | 32 | 32 | 32 | 32 | 32 | (mm) |
| 26. R28k A7 | 250 | 50 | 36 | 32 | 30 | 30 | 30 | 30 | 30 | 30 | (mm) |
| 27. R12 A6 | 250 | 170 | 70 | 36 | 29 | 26 | 26 | 26 | 26 | 26 | (mm) |
| 28. R22 A23 | 250 | 130 | 46 | 38 | 32 | 29 | 29 | 29 | 29 | 29 | (mm) |
| 29. R1 A2 | 250 | 60 | 41 | 37 | 34 | 32 | 32 | 32 | 32 | 32 | (mm) |
| 30. R6 A34 | 250 | 54 | 39 | 35 | 32 | 30 | 30 | 30 | 30 | 30 | (mm) |
| 31. R25 A29 | | | | | | | | | | | |

Table 14: The classification of the adherent anode slime samples into settling rate groups, based on sediment column heights. The samples with clear supernatants after 10 minutes have been underlined.

| Slow | Intermediate | Fast |
|---|---|---|
| | 1. R24s A19 | |
| | 2. R11 A7 | |
| | 3. R24k A11 | |
| 4. R20 A30 | | |
| | 6. R8 A2 | |
| | 7. R17 A17 | |
| | 8. R9 A20 | |
| 9. R28s A34 | | |
| | 10. R7 A5 | |
| | 11. R23 A16 | |
| | | 12. R18 A24 |
| | | 13. R2 A4 |
| | 14. R15 A3 | |
| | | 15. R3 A4 |
| | 17. R10 A14 | |
| | | 18. R5 A15 |
| | 19. R19 A7 | |
| | 20. R4 A4 | |
| | | 21. R26 A25 |
| | | 22. R21 A4 |
| | | 23. R14 A9 |
| | | 25. R16 A16 |
| | | 26. R28k A7 |
| | 27. R12 A6 | |
| | 28. R22 A23 | |
| | | 29. R1 A2 |
| | | 30. R6 A34 |

## 4.2 Particle size distributions

The results of the particle size distribution analyses are presented in table 15, which shows the values of d(0.1), d(0.5) and d(0.9) of each adherent anode slime sample. Table 15 includes the "tail" areas of the particle size distributions, also. Figures 25, 26 and 27 show the frequency curves of samples 9. R28s A34, 11. R23 A16 and 25. R16 A16, respectively. As explained in more detail in chapter 4.1 Moisture contents and settling, these samples represent different adherent anode slime settling rate groups.

In despite of the different settling rates, the frequency curves of the three samples appear to be quite similar. In the graphs, the most detectable differences are the "tails" of the samples 9. R28s A34 and 11. R23 A16. In the graph of sample 9. R28s A34, two out of three measurements show a "tail" around 100 $\mu$m. In the graph of sample 11. R23 A16, one measurement out of three shows a "tail" around 100-200 $\mu$m. However, upon further examination of table 15, the values of d(0.1), d(0.5) and d(0.9) of the samples are quite different, although the values of d(0.1) and d(0.9) of samples 11. R23 A16 and 25. R16 A16 show similarity.

From table 15 it can also be seen that the values of d(0.1) and of d(0.5) are quite similar for samples 4. R20 A30 and 9. R28s A34. These two samples have the slowest settling rates, as can be seen from tables 13 and 14. Contrary to expectations, other correlations between the the particle size distributions and the settling rates of the adherent anode slime samples are not easily found. This might be due to the fact that ultrasound was used to break up possible agglomerates in the particle size distribution measurements but not in the settling tests.

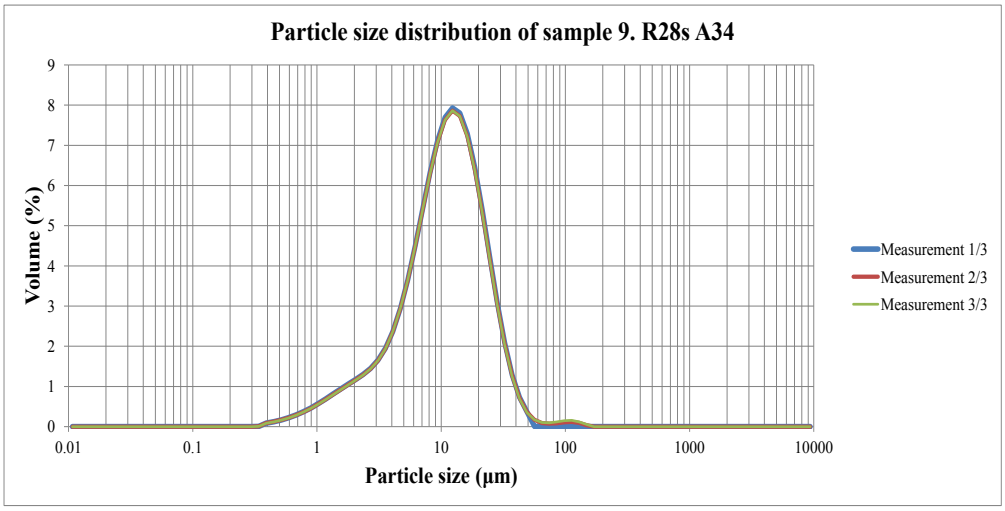


Figure 25: The particle size distribution of sample 9. R28s A34.

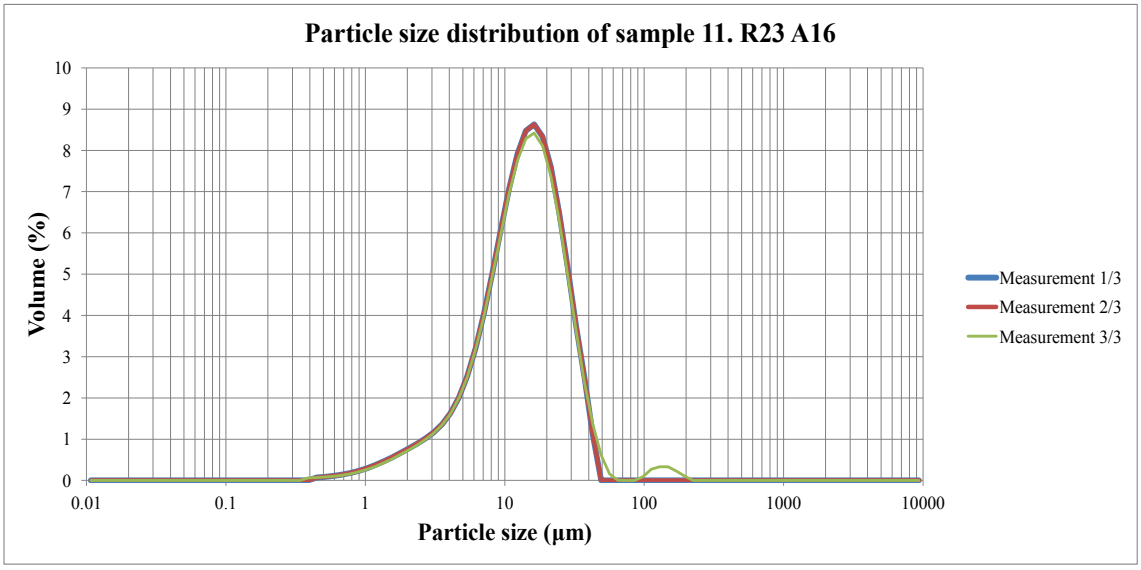


Figure 26: The particle size distribution of sample 11. R23 A16

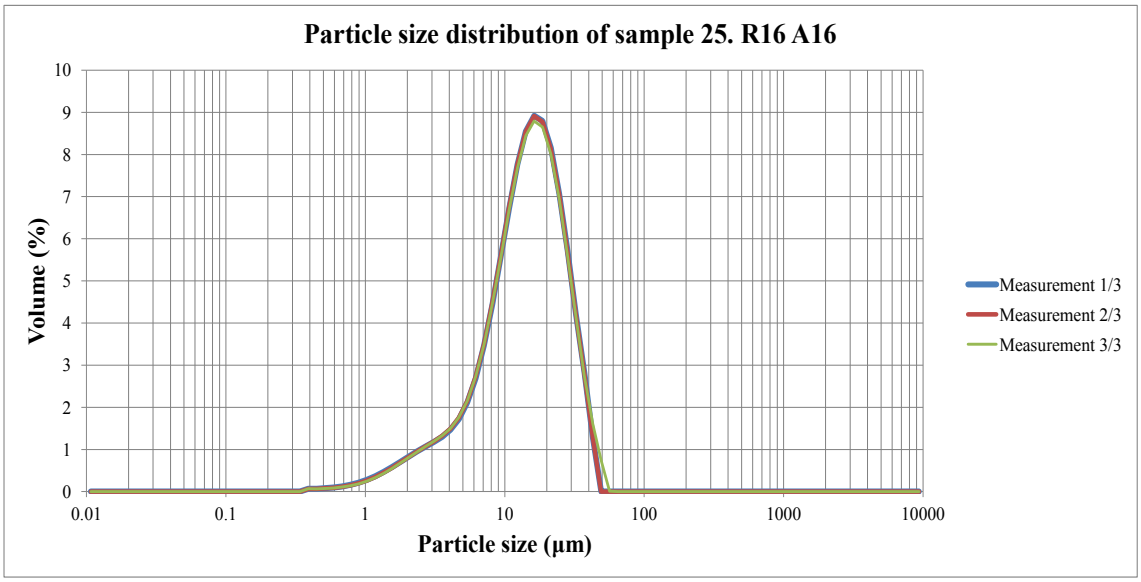


Figure 27: The particle size distribution of sample 25. R16 A16.

Table 15: The particle size distribution analysis results of the adherent anode slime samples. The results of sample 5. R13 A8 are in paranthesis due to result unreliability. The results of samples 9. R28s A34, 11. R23 A16 and 25. R16 A16 have been emphasized.

| Sample | d(0.1) ($\mu$m) | d(0.5) ($\mu$m) | d(0.9) ($\mu$m) | "Tail" area ($\mu$m) |
|---|---|---|---|---|
| 1. R24s A19 | 3.85 | 14.03 | 28.78 | |
| 2. R11 A7 | 4.01 | 14.12 | 31.03 | |
| 3. R24k A11 | 4.27 | 14.85 | 31.31 | |
| 4. R20 A30 | 2.84 | 10.56 | 37.47 | 100-700 |
| 5. R13 A8 | (3.56) | (14.92) | (46.79) | (300-700) |
| 6. R8 A2 | 2.61 | 10.66 | 29.03 | 100-200 |
| 7. R17 A17 | 4.36 | 14.05 | 30.53 | |
| 8. R9 A20 | 4.52 | 14.56 | 29.78 | |
| **9. R28s A34** | **2.99** | **10.89** | **24.79** | **100** |
| 10. R7 A5 | 3.59 | 10.61 | 24.29 | |
| **11. R23 A16** | **4.47** | **13.87** | **29.75** | **100-200** |
| 12. R18 A24 | 4.16 | 13.51 | 27.03 | |
| 13. R2 A4 | 3.86 | 13.66 | 27.29 | |
| 14. R15 A3 | 3.17 | 12.01 | 28.22 | 100 |
| 15. R3 A4 | 4.09 | 13.45 | 26.92 | |
| 16. R27k A25 | 3.99 | 11.74 | 24.99 | |
| 17. R10 A14 | 4.10 | 12.53 | 31.89 | |
| 18. R5 A15 | 4.66 | 14.94 | 29.79 | |
| 19. R19 A7 | 4.36 | 13.50 | 27.77 | |
| 20. R4 A4 | 4.27 | 14.69 | 36.61 | 100-300 |
| 21. R26 A25 | 4.45 | 14.70 | 29.94 | |
| 22. R21 A4 | 4.07 | 12.59 | 28.70 | 100-200 |
| 23. R14 A9 | 4.38 | 15.38 | 30.49 | |
| 24. R27s A7 | 3.97 | 13.78 | 28.91 | |
| **25. R16 A16** | **4.44** | **14.48** | **29.59** | |
| 26. R28k A7 | 4.12 | 14.63 | 29.71 | |
| 27. R12 A6 | 3.77 | 13.62 | 32.97 | 100-700 |
| 28. R22 A23 | 3.59 | 12.84 | 27.34 | |
| 29. R1 A2 | 4.13 | 13.99 | 29.07 | |
| 30. R6 A34 | 3.99 | 14.74 | 30.26 | |
| 31. R25 A29 | 2.61 | 9.61 | 21.04 | |

## 4.3 Chemical analysis

The chemical analysis of the anodes and the adherent anode slimes are presented in tables 19 and 20, respectively. The impurity concentrations of table 19 are not sample specific, but represent instead the average values of the anode lots within a group (R). The group of a sample can consist of more than two anode lots with different anode compositions and during the making of the thesis it was not possible to connect the anode lug sample with the corresponding anode lot. The adherent anode slime impurity element concentrations in table 20, on the other hand, are sample specific.

With the available methods, it was not possible to analyse the concentration of oxygen from the adherent anode slimes. Hence, the oxygen concentrations of the adherent anode slimes are missing from table 20. However, table 20 does include the adherent anode slime copper concentrations. In both tables 19 and 20, the highest nickel concentrations have been emphasized due to reasons discussed in more detail in chapter 4.4 XRD analysis.

The average concentrations and the corresponding standard deviations and percentage errors of the impurities in the anodes and in the adherent anode slimes are presented in tables 16 and 17, respectively. In table 16, the impurity element average concentrations and the standard deviations have been calculated from the values of table 19. Similarly, the values of table 17 have been calculated from the values of table 20.

Table 16: The average concentrations, corresponding standard deviations and percentage errors of the impurity elements in the anodes. "Bal." stands for balance, which means that the rest of the anodes (≈99 %) is copper.

| Impurity element | Average concentration (ppm) | Standard deviation (ppm) | Error (%) |
|---|---|---|---|
| Cu | Bal. | | |
| Ni | 3045.16 | 625.19 | 20.53 |
| As | 2478.26 | 249.75 | 10.08 |
| $O_2$ | 1919.35 | 238.84 | 12.44 |
| Ag | 1414.84 | 129.67 | 9.17 |
| Pb | 664.58 | 88.96 | 13.39 |
| Se | 606.35 | 54.53 | 8.99 |
| Bi | 534.52 | 76.61 | 14.33 |
| Sb | 491.42 | 154.41 | 31.42 |
| Te | 246.65 | 63.72 | 25.83 |

Table 17: The average concentrations, corresponding standard deviations and percentage errors of the impurity elements in the adherent anode slimes. The standard deviations are presented as percentage points (pp).

| Impurity element | Average concentration (%) | Standard deviation (pp) | Error (%) |
|---|---|---|---|
| Ag | 21.05 | 3.60 | 17.11 |
| Cu | 17.70 | 5.16 | 29.16 |
| Pb | 8.35 | 2.15 | 25.68 |
| Se | 6.48 | 2.15 | 33.24 |
| Bi | 5.48 | 2.30 | 41.98 |
| As | 5.40 | 1.06 | 19.54 |
| Sb | 3.73 | 0.83 | 22.36 |
| Ni | 2.96 | 3.84 | 129.95 |
| Te | 1.50 | 1.15 | 76.86 |

The standard deviation expresses how much the concentrations of a certain impurity element vary from the average concentrations. The higher the value of standard deviation is, the more there is variation in the specific impurity element concentrations in the samples. The percentage error has been calculated by dividing the standard deviation values by the average concentrations. The percentage error can be used to compare the variations of different impurity element concentrations in the samples.

According to the percentage error values of table 16, the concentrations of silver vary the least and the concentrations of bismuth the most in the anodes. The percentage error values of table 17 show that in the adherent anode slime samples also, the concentrations of silver vary the least. In the adherent anode slime samples, the concentrations of nickel vary the most.

The correlation factors of the anode impurity elements and the corresponding adherent anode slime impurity elements are presented in table 18. The table 18 shows that the nickel concentrations in the anodes and in the adherent anode slimes have the strongest correlation. Interestingly, in the same table, bismuth has a slight negative correlation. This would indicate that as the concentration of bismuth increases in the anodes, it decreases in the adherent anode slimes. In their research, Möller et al. (2010) claim that since a fixed amount of bismuth is bound as insoluble and complex oxides, decreasing amounts of bismuth report to the anode slimes at higher concentrations of bismuth in the anodes.

Table 18: The correlation factors between anode and adherent anode slime impurity elements. Correlation factor value "1" would indicate direct proportionality and value "-1" inverse proportionality.

| Impurity element | Correlation factor |
|---|---|
| Ni | 0.63 |
| Te | 0.56 |
| Pb | 0.51 |
| Ag | 0.29 |
| As | 0.18 |
| Se | 0.17 |
| Sb | 0.16 |
| Bi | -0.19 |

Table 19: The chemical analysis of the anodes. The presented impurity element concentrations are average concentrations of the anode lots within the group. Nickel concentrations higher than 3000 ppm appear with a bolder font. The highest nickel concentrations of the samples have been underlined.

| Sample | Ag | Pb | As | Sb | Bi | Ni | Te | Se | $O_2$ | (ppm) |
|---|---|---|---|---|---|---|---|---|---|---|
| 1. R24s A19 | 1676 | 717 | 2234 | 409 | 498 | **3000** | 223 | 586 | 1700 | |
| 2. R11 A7 | 1673 | 754 | 2415 | 420 | 486 | **3400** | 210 | 587 | 1600 | |
| 3. R24k A11 | 1595 | 682 | 2685 | 414 | 504 | **3500** | 213 | 592 | 1900 | |
| 4. R20 A30 | 1522 | 626 | 2650 | 398 | 496 | **3400** | 220 | 592 | 1800 | |
| 5. R13 A8 | 1594 | 658 | 2733 | 448 | 538 | **3400** | 227 | 596 | 1600 | |
| 6. R8 A2 | 1390 | 595 | 2411 | 361 | 483 | **3200** | 225 | 558 | 1700 | |
| 7. R17 A17 | 1423 | 659 | 2571 | 387 | 500 | **3900** | 229 | 593 | 1600 | |
| 8. R9 A20 | 1518 | 757 | 2781 | 433 | 537 | **5000** | 262 | 694 | 1600 | |
| 9. R28s A34 | 1501 | 852 | 2343 | 407 | 563 | **4300** | 220 | 635 | 2100 | |
| 10. R7 A5 | 1442 | 843 | 2198 | 379 | 534 | **3800** | 224 | 630 | 1900 | |
| 11. R23 A16 | 1322 | 724 | 2267 | 375 | 563 | **3400** | 201 | 613 | 1900 | |
| 12. R18 A24 | 1324 | 849 | 2058 | 379 | 529 | **3600** | 190 | 609 | 2000 | |
| 13. R2 A4 | 1316 | 636 | 2119 | 345 | 518 | 2900 | 205 | 559 | 1900 | |
| 14. R15 A3 | 1262 | 621 | 2727 | 372 | 565 | 2800 | 227 | 585 | 1900 | |
| 15. R3 A4 | 1229 | 511 | 2201 | 323 | 458 | 2900 | 203 | 547 | 1900 | |
| 16. R27k A25 | 1110 | 686 | 2546 | 351 | 458 | **3200** | 221 | 611 | 1900 | |
| 17. R10 A14 | 1110 | 686 | 2546 | 351 | 458 | **3200** | 221 | 611 | 1900 | |
| 18. R5 A15 | 1300 | 623 | 2586 | 384 | 419 | 2400 | 166 | 610 | 1900 | |
| 19. R19 A7 | 1336 | 643 | 2878 | 478 | 463 | 2700 | 220 | 609 | 2100 | |
| 20. R4 A4 | 1372 | 675 | 2966 | 778 | 550 | 2700 | 329 | 738 | 2000 | |
| 21. R26 A25 | 1383 | 647 | 2767 | 786 | 584 | 2600 | 359 | 721 | 2100 | |
| 22. R21 A4 | 1431 | 607 | 2436 | 855 | 701 | 2400 | 457 | 724 | 2800 | |
| 23. R14 A9 | 1347 | 604 | 2069 | 528 | 524 | 2700 | 320 | 540 | 2100 | |
| 24. R27s A7 | 1313 | 509 | 2102 | 488 | 575 | 2800 | 328 | 537 | 2300 | |
| 25. R16 A16 | 1404 | 570 | 2300 | 542 | 633 | **3100** | 301 | 574 | 2100 | |
| 26. R28k A7 | 1420 | 624 | 2330 | 574 | 645 | **3100** | 284 | 583 | 2000 | |
| 27. R12 A6 | 1455 | 540 | 2706 | 769 | 720 | 2400 | 330 | 692 | 1700 | |
| 28. R22 A23 | 1562 | 657 | 2619 | 732 | 633 | 2300 | 258 | 571 | 1900 | |
| 29. R1 A2 | 1558 | 683 | 2692 | 749 | 609 | 2300 | 259 | 587 | 1800 | |
| 30. R6 A34 | 1483 | 811 | 2499 | 540 | 437 | 2500 | 177 | 513 | 1700 | |
| 31. R25 A29 | 1319 | 586 | 2467 | 488 | 447 | 2300 | 202 | 596 | 2100 | |

Table 20: The chemical analysis of the adherent anode slime samples. High nickel concentrations have been underlined.

| Sample | Ag | Pb | As | Sb | Bi | Ni | Te | Se | Cu | (%) |
|---|---|---|---|---|---|---|---|---|---|---|
| 1. R24s A19 | 20.80 | 10.60 | 5.40 | 2.48 | 3.48 | 2.32 | 0.20 | 3.91 | 21.50 | |
| 2. R11 A7 | 23.80 | 11.10 | 5.22 | 3.34 | 4.52 | 1.93 | 0.10 | 4.18 | 15.30 | |
| 3. R24k A11 | 24.70 | 7.66 | 5.40 | 2.47 | 2.77 | 0.60 | 0.42 | 4.86 | 23.20 | |
| 4. R20 A30 | 27.00 | 10.60 | 4.67 | 3.60 | 5.99 | 1.85 | 0.32 | 5.51 | 10.50 | |
| 5. R13 A8 | 19.00 | 7.52 | 7.55 | 3.67 | 4.00 | 3.98 | 0.21 | 4.06 | 14.40 | |
| 6. R8 A2 | 24.80 | 7.80 | 5.03 | 4.30 | 6.50 | 4.02 | 0.41 | 5.49 | 10.70 | |
| 7. R17 A17 | 14.80 | 7.36 | 4.12 | 2.97 | 4.20 | 12.58 | 0.07 | 3.28 | 12.10 | |
| 8. R9 A20 | 16.90 | 6.74 | 5.60 | 3.13 | 5.07 | 8.81 | 0.18 | 3.85 | 15.00 | |
| 9. R28s A34 | 18.70 | 13.30 | 3.79 | 2.83 | 4.16 | 11.42 | 0.12 | 4.15 | 6.38 | |
| 10. R7 A5 | 17.20 | 11.70 | 5.35 | 3.28 | 4.16 | 11.25 | 0.12 | 3.91 | 9.69 | |
| 11. R23 A16 | 15.80 | 6.45 | 5.57 | 4.49 | 5.75 | 7.74 | 0.03 | 3.43 | 17.20 | |
| 12. R18 A24 | 15.80 | 13.10 | 5.97 | 2.89 | 4.12 | 1.99 | 0.49 | 4.31 | 21.30 | |
| 13. R2 A4 | 23.10 | 9.81 | 5.43 | 2.73 | 3.29 | 0.28 | 0.85 | 5.22 | 22.00 | |
| 14. R15 A3 | 23.10 | 9.69 | 5.34 | 3.78 | 7.62 | 1.09 | 1.86 | 8.39 | 14.10 | |
| 15. R3 A4 | 18.30 | 8.72 | 6.78 | 4.25 | 8.31 | 0.65 | 1.48 | 6.45 | 20.10 | |
| 16. R27k A25 | 20.10 | 7.73 | 7.24 | 5.74 | 12.70 | 0.46 | 2.36 | 9.44 | 14.20 | |
| 17. R10 A14 | 16.50 | 7.30 | 6.07 | 5.65 | 11.50 | 10.80 | 1.40 | 5.31 | 10.60 | |
| 18. R5 A15 | 18.50 | 6.76 | 7.01 | 3.90 | 7.20 | 0.48 | 1.93 | 7.67 | 23.30 | |
| 19. R19 A7 | 20.10 | 8.00 | 6.66 | 4.15 | 7.20 | 0.37 | 2.33 | 8.17 | 18.90 | |
| 20. R4 A4 | 22.90 | 7.72 | 5.84 | 3.89 | 5.90 | 0.43 | 1.95 | 9.15 | 19.80 | |
| 21. R26 A25 | 17.40 | 7.97 | 6.44 | 4.99 | 7.02 | 1.42 | 2.16 | 7.06 | 21.20 | |
| 22. R21 A4 | 23.40 | 7.95 | 4.13 | 3.96 | 4.11 | 1.11 | 2.98 | 9.62 | 19.30 | |
| 23. R14 A9 | 20.00 | 5.08 | 5.20 | 2.77 | 3.11 | 0.57 | 3.60 | 8.28 | 29.20 | |
| 24. R27s A7 | 23.60 | 7.29 | 3.91 | 3.47 | 3.91 | 0.70 | 3.15 | 7.83 | 20.20 | |
| 25. R16 A16 | 20.40 | 6.54 | 5.00 | 3.22 | 4.30 | 0.68 | 2.71 | 6.84 | 25.40 | |
| 26. R28k A7 | 18.30 | 5.22 | 6.48 | 4.95 | 7.47 | 1.19 | 2.28 | 7.00 | 22.80 | |
| 27. R12 A6 | 24.50 | 6.88 | 4.17 | 4.48 | 6.04 | 1.07 | 3.31 | 10.30 | 16.50 | |
| 28. R22 A23 | 26.30 | 6.92 | 4.10 | 3.96 | 4.17 | 0.62 | 3.03 | 9.64 | 17.70 | |
| 29. R1 A2 | 27.20 | 5.12 | 5.34 | 3.52 | 3.59 | 0.28 | 2.36 | 7.20 | 21.40 | |
| 30. R6 A34 | 22.70 | 8.95 | 5.52 | 3.81 | 3.77 | 0.63 | 1.83 | 6.60 | 21.20 | |
| 31. R25 A29 | 26.80 | 11.40 | 3.17 | 3.06 | 3.81 | 0.35 | 2.19 | 9.76 | 13.60 | |

## 4.4 XRD analysis

The results of the XRD analysis are presented in table 21, which presents a score for each species of interest. The score values were calculated by PANalytical X'Pert Highscore Plus software, which compares the peak positions and intensities of the sample spectrum with the impurity species reference peaks. Therefore, the species in question are more likely to be found in the adherent anode slime sample if their score values are high.

In table 21, letter "N" stands for "No matching lines" and letter "U" for "Unmatched strong". The PANalytical X'Pert Highscore Plus software presents the former message when it cannot find correlation between the peaks of the sample spectrum and the reference peaks of the species. The latter message is presented when at least one of the strong reference peaks (> 50 %) of the impurity species does not appear in the sample spectrum.

Figures 28 and 29 present the XRD spectrums of samples 9. R28s A34 and 25. R16 A16, respectively, before the analysis. Figures 30 and 31 show the same sample spectrums with the impurity species reference peaks included. The reference peaks of the chosen impurity species seem to match quite well with the sample spectrum peaks. However, it would appear that the peaks of $Ag_2Se$ have shifted slightly in all of the sample spectrums. Also, almost all of the sample spectrums systematically contain three peaks that cannot be explained with the chosen impurity species' reference peaks. The $2\theta$ values of these peaks are between 17.55-18.38, 28.19-28.38 and 30.28-30.66.

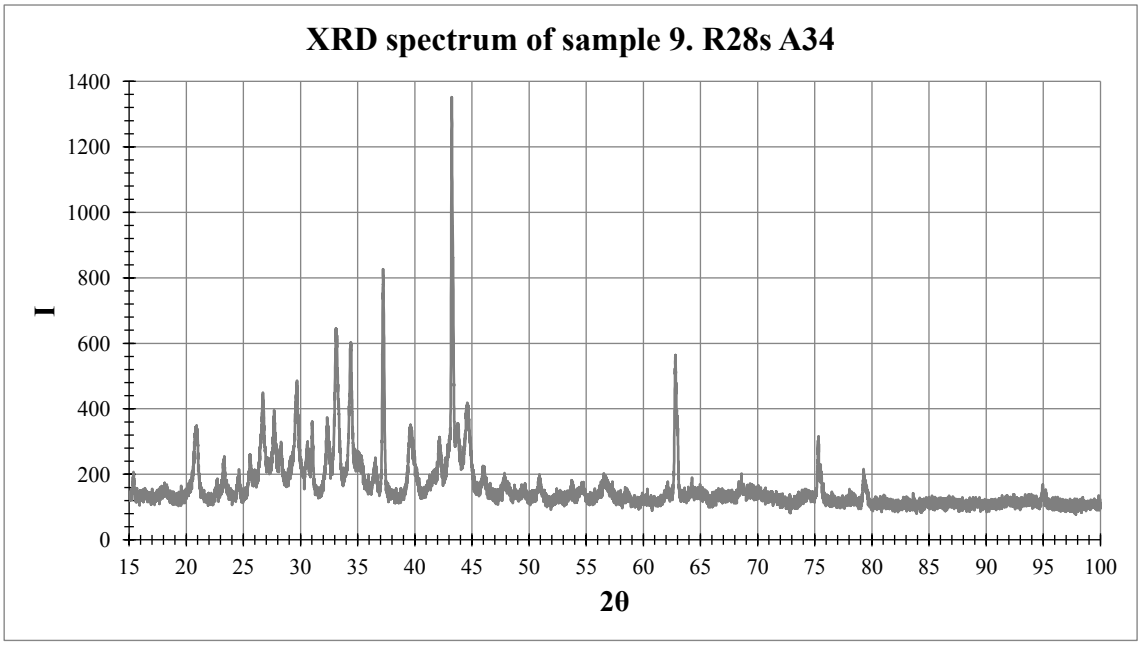


Figure 28: The XRD spectrum of sample 9. R28s A34.

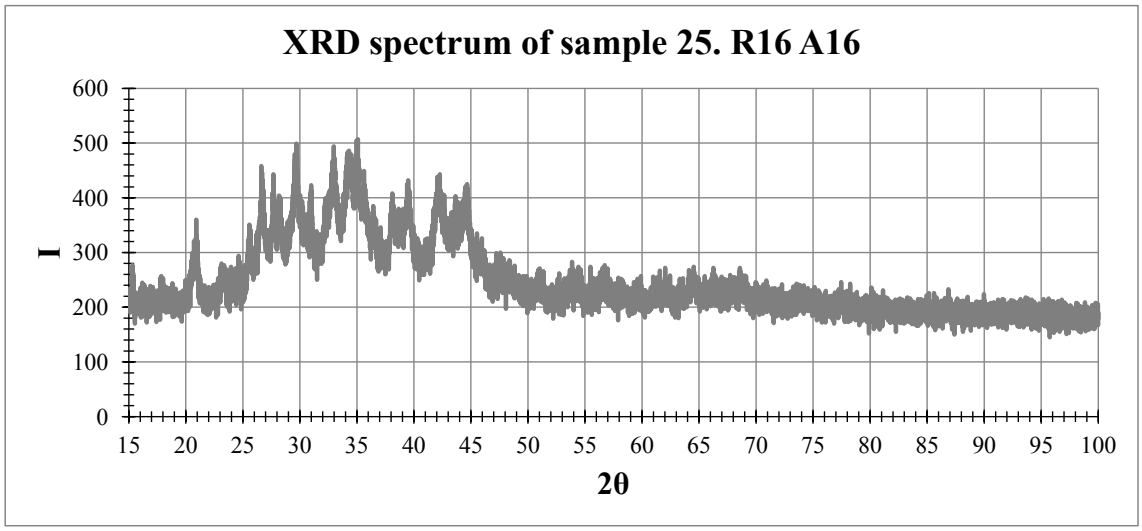


Figure 29: The XRD spectrum of sample 25. R16 A16.

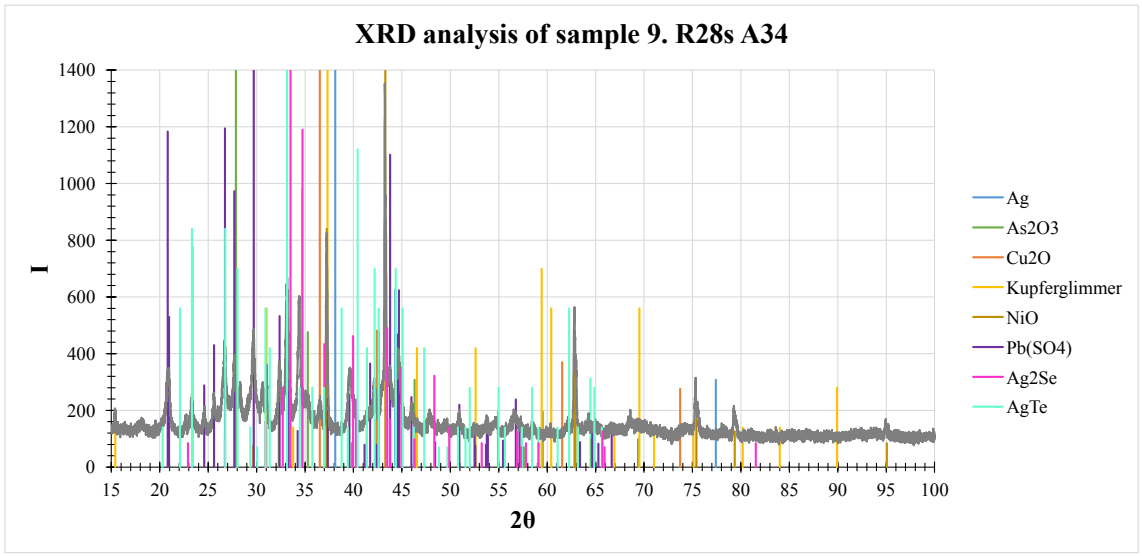


Figure 30: The XRD spectrum of sample 9. R28s A34 with the impurity species' reference peaks.

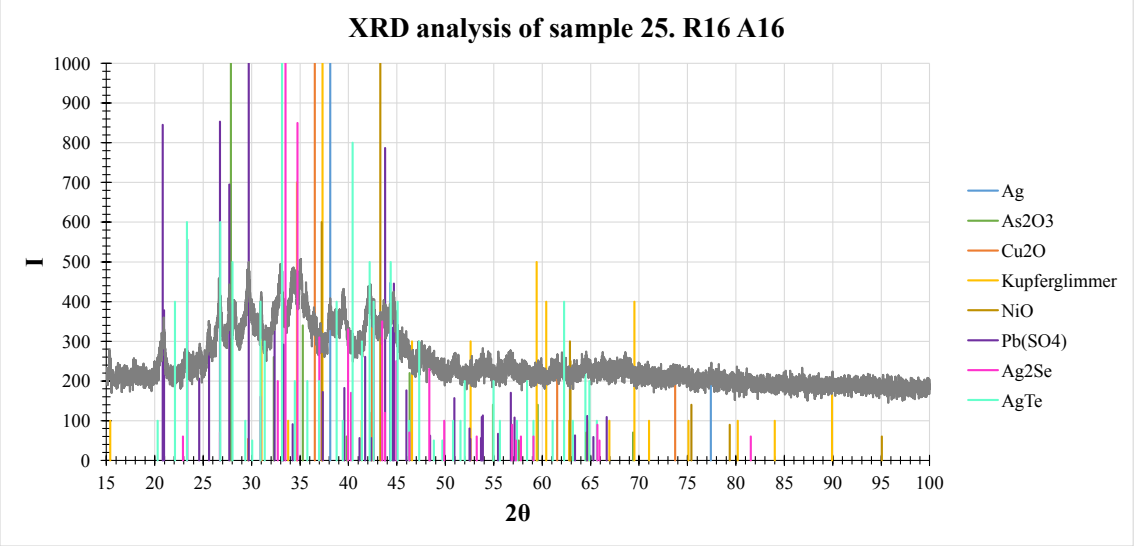


Figure 31: The XRD spectrum of sample 25. R16 A16 with the impurity species' reference peaks.

The XRD analysis results of $CuSO_4$ are not included in table 21, since the score value for all the samples was "Unmatched strong". From table 21 it can be seen that the scores of $Cu_2O$ are also low for most of the samples. The low scores of these two species could indicate unsuitable conditions for the formation of non-conducting films and for anode passivation. This is in line with the fact that anode passivation has not been a problem at the Boliden Pori electrorefinery.

The only species that scores high in all of the samples is $PbSO_4$. Therefore, it is very likely that $PbSO_4$ is present in all the adherent anode slime samples. This correlates with the data found in literature (Chen & Dutrizac, 1990b; Moats et al. 2012), according to which almost all of the lead in the anodes dissolves and then precipitates on the anode surface as $PbSO_4$ observed in the XRD analysis.

In table 21, the highest scores of NiO ($\geq$ 40) and kupferglimmer ($\geq$ 9) are in samples 7. R17 A17, 8. R9 A20, 9. R28s A34, 10. R7 A5, 11. R23 A16, and 17. R10 A14. The same samples have high nickel concentrations in table 20, presenting the chemical analyses of the adherent anode slimes. Also in table 19, in despite of presenting anode lot average impurity concentrations, samples 7. R17 A17, 8. R9 A20, 9. R28s A34 and 10. R7 A5 have the highest nickel concentrations ($\geq$ 3800 ppm) out of all the samples.

As mentioned in literature (Forsén, 1985), NiO can form even with low oxygen content (0.1 wt-%) if nickel concentration exceeds 0.32 wt-%. Also the antimony concentration

(200 ppm) required for kupferglimmer to form (Chen & Dutrizac, 1989b) is exceeded in all of the anodes. Therefore, the nickel concerning data in tables 21, 20 and 19 seems to be in line with literature (Forsén, 1985; Chen & Dutrizac, 1990a; 1989b), what comes to NiO and kupferglimmer formation and deportment into the slimes.

Table 21: The scores of different impurity species, from the XRD spectrums. "N" stands for "No matching lines" and "U" for "Unmatched strong".

| Sample | $Cu_2O$ | Ag | $PbSO_4$ | $As_2O_3$ | NiO | Kupferglimmer | $Ag_2Se$ | AgTe |
|---|---|---|---|---|---|---|---|---|
| 1. R24s A19 | 33 | 39 | 36 | 16 | 27 | 4 | 7 | 10 |
| 2. R11 A7 | 1 | 45 | 36 | 10 | 13 | U | 6 | 10 |
| 3. R24k A11 | 0 | 47 | 29 | 0 | 4 | 2 | 6 | 10 |
| 4. R20 A30 | 10 | 3 | 28 | 8 | 16 | 7 | 16 | 9 |
| 5. R13 A8 | (6) | (N) | (16) | (24) | (34) | (9) | (17) | (U) |
| 6. R8 A2 | 4 | 3 | 26 | 5 | 37 | 6 | 2 | 8 |
| 7. R17 A17 | 1 | 4 | 35 | 10 | 50 | 8 | U | 14 |
| 8. R9 A20 | 0 | 3 | 36 | 0 | 47 | 8 | 9 | 13 |
| 9. R28s A34 | 12 | 4 | 36 | 13 | 47 | 8 | 13 | 12 |
| 10. R7 A5 | 12 | 3 | 31 | 4 | 47 | 9 | 15 | 11 |
| 11. R23 A16 | 1 | 9 | 26 | 4 | 44 | 9 | 7 | 8 |
| 12. R18 A24 | 1 | 9 | 38 | 2 | 12 | 2 | 7 | 12 |
| 13. R2 A4 | 17 | 4 | 35 | 2 | 5 | 1 | 6 | 9 |
| 14. R15 A3 | 6 | 4 | 31 | 7 | 8 | 2 | 6 | 13 |
| 15. R3 A4 | 3 | 10 | 30 | 1 | 2 | U | 5 | 12 |
| 16. R27k A25 | 1 | 1 | 27 | 4 | N | U | 7 | U |
| 17. R10 A14 | 1 | 2 | 29 | 7 | 40 | 8 | 11 | 11 |
| 18. R5 A15 | 0 | 8 | 34 | 0 | 3 | U | 8 | 14 |
| 19. R19 A7 | 1 | 16 | 28 | 3 | 8 | 1 | 12 | 13 |
| 20. R4 A4 | 4 | 20 | 27 | 3 | 8 | 1 | 8 | 11 |
| 21. R26 A25 | 0 | 24 | 26 | 6 | 3 | 1 | 15 | 11 |
| 22. R21 A4 | 3 | 4 | 27 | 4 | 7 | 3 | 11 | 11 |
| 23. R14 A9 | 30 | 3 | 23 | 1 | N | U | 8 | 10 |
| 24. R27s A7 | 2 | 1 | 19 | 2 | N | 2 | 1 | 7 |
| 25. R16 A16 | 1 | 11 | 15 | 2 | N | 1 | U | U |
| 26. R28k A7 | 22 | 5 | 17 | 3 | 5 | U | 4 | U |
| 27. R12 A6 | 3 | 4 | 21 | 5 | 5 | U | 1 | U |
| 28. R22 A23 | 3 | 5 | 17 | 3 | 3 | 2 | 13 | U |
| 29. R1 A2 | 0 | 18 | 11 | 1 | N | U | 1 | U |
| 30. R6 A34 | 2 | 33 | 26 | 2 | 5 | 2 | 10 | U |
| 31. R25 A29 | 5 | 5 | 37 | 7 | 14 | 3 | 17 | 16 |

## 4.5 SEM and anode micrographs

The morphologies of the dried adherent anode slime samples 14. R15 A3 and 23. R14 A9 with the most and the least impurities based on chemical analysis, are presented in figure 32, in three different scales. No significant differences in the adherent anode slime morphologies can be observed, which might be due to $PbSO_4$.

Figures 33, 34 and 35 present the microstructures of anode lug samples 14. R15 A3, 23. R14 A9 and 31. R25 A28, respectively. Figure 33 presents two 5x magnifications of the micrograph, showing two interesting microstructures types. Figures 34 and 35 show 5x and 20x magnifications of the anode microstructures. Judging from the 5x magnifications (left hand side) of figures 33 and 34, the microsturctures seem fairly similar.

In figure 35, well formed crystalline impurities can be observed. In literature (Forsén, 1985; Chen & Dutrizac, 1990a), crystalline impurities with a similar shape have been identified as NiO crystals. Due to this observation, the anode micrographs have been divided into two groups based on their nickel contents in table 22. The division has been made based on the nickel concentrations of table 19. Interestingly, out of the five micrographs that clearly contain the crystalline impurities similar to those in figure 35, only one has a nickel concentration higher than 0.3 %.

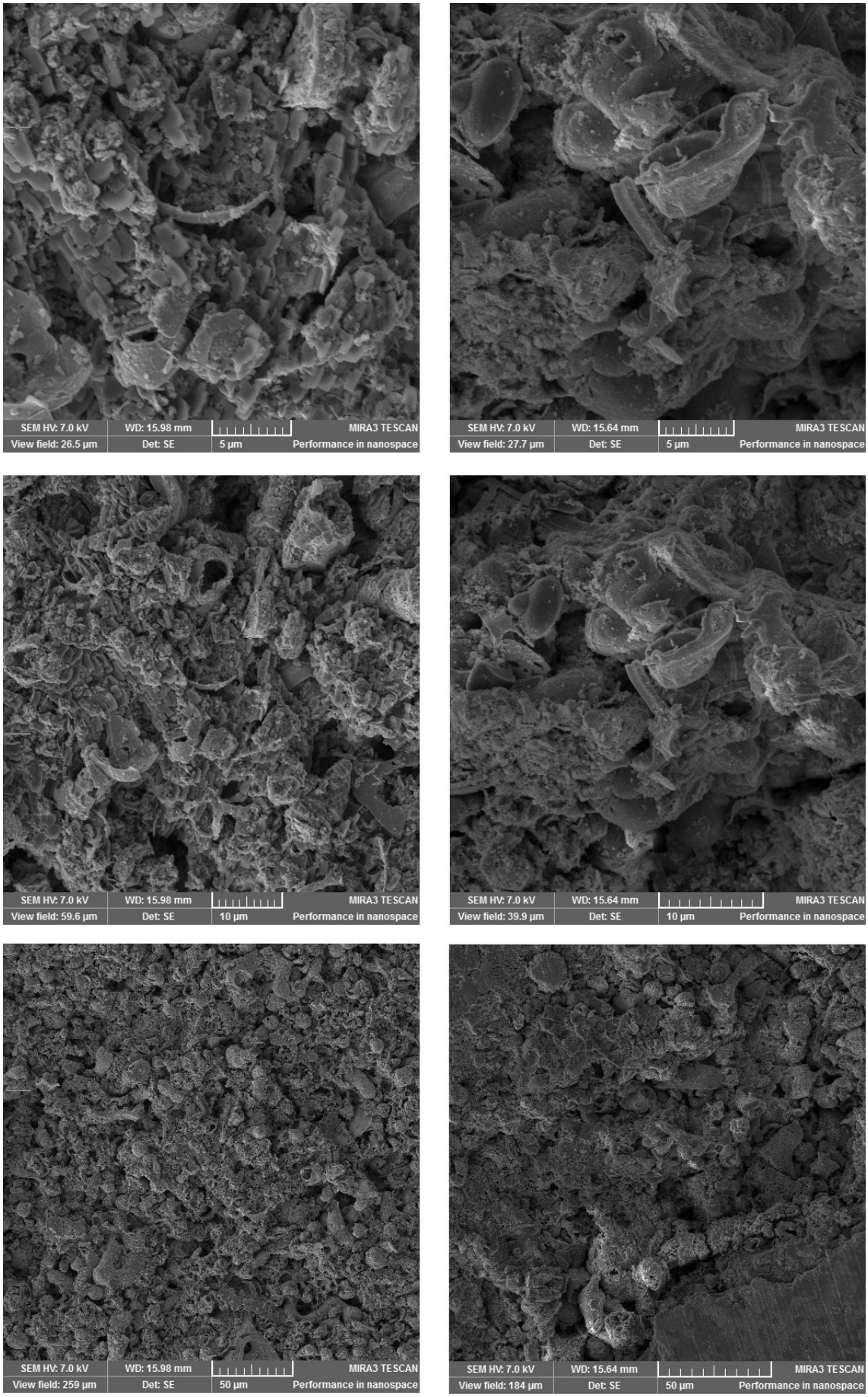




Figure 32: On the left, the surface morphology of sample 14. R15 A3, containing the most impurities. On the right, the surface morphology of sample 23. R14 A9, containing the least impurities.

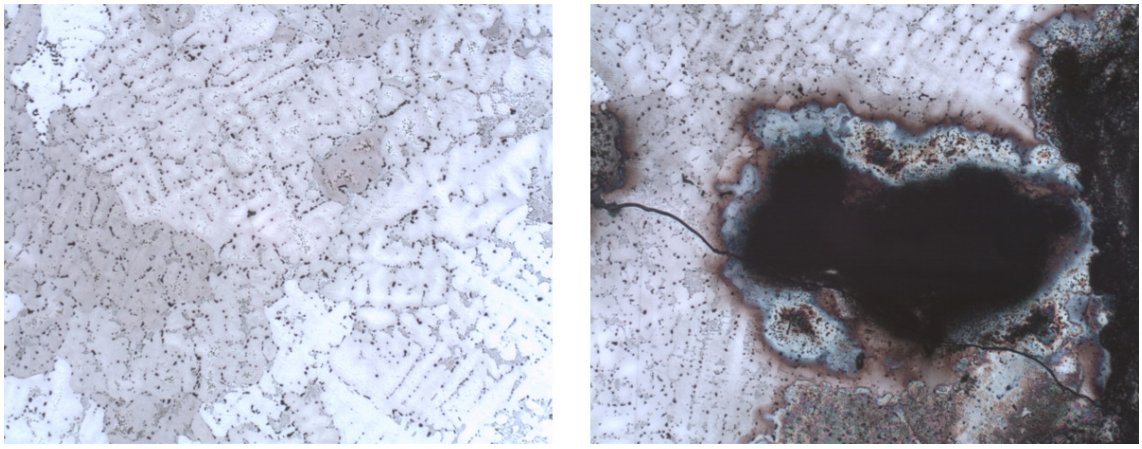

Figure 33: The microstructure of anode sample 14. R15 A3. On the left, 5x magnification of the bulk microstructure. On the right, 5x magnification of a cavity in the microstructure.

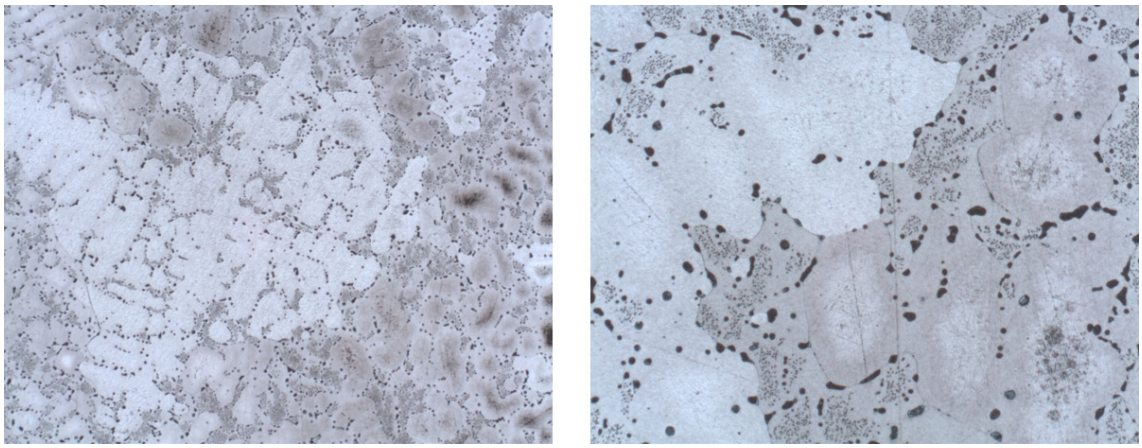

Figure 34: The microstructure of anode sample 23. R14 A9. On the left, 5x magnification. On the right, 20x magnification.

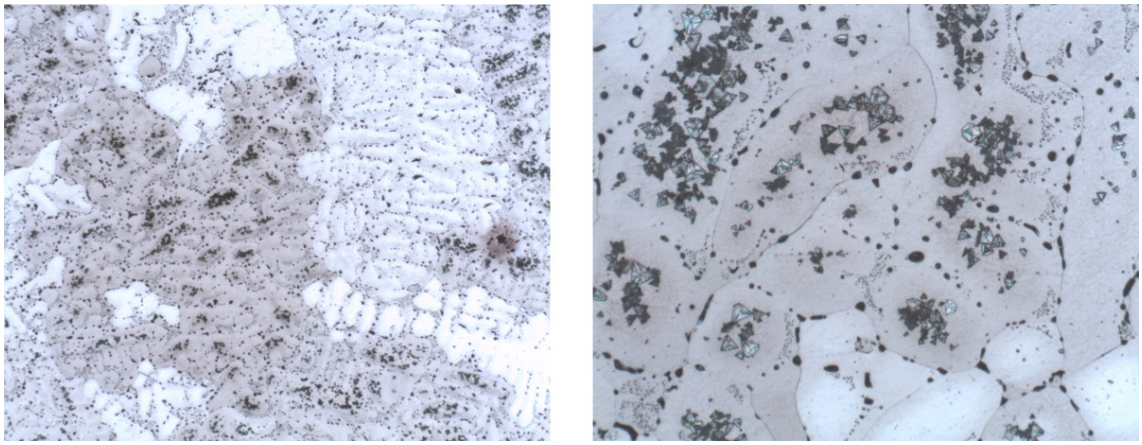

Figure 35: The microstructure of anode sample 31. R25 A28. On the left, 5x magnification. On the right, 20x magnification with the possible NiO crystals clearly visible.

Table 22: Anode microstructure categorization, based on nickel concentration. The micrographs showing well formed, possibly NiO crystals have been underlined.

| Ni $\geq$ 0.3 % | Ni < 0.3 % |
|---|---|
| 1. R24s A19 | |
| 2. R11 A7 | |
| 3. R24k A11 | |
| 4. R20 A30 | |
| 5. R13 A18 | |
| 6. R8 A2 | |
| 7. R17 A17 | |
| 8. R9 A20 | |
| 9. R28s A34 | |
| 10. R7 A5 | |
| 11. R23 A16 | |
| 12. R18 A24 | |
| | 13. R2 A4 |
| | 14. R15 A3 |
| | 15. R3 A4 |
| 16. R27k A25 | |
| 17. R10 A14 | |
| | 18. R5 A15 |
| | 19. R19 A7 |
| | 20. R4 A4 |
| | 21. R26 A25 |
| | 22. R21 A4 |
| | 23. R14 A9 |
| | 24. R27s A7 |
| 25. R16 A16 | |
| 26. R28k A7 | |
| | 27. R12 A6 |
| | 28. R22 A23 |
| | 29. R1 A2 |
| | 30. R6 A34 |
| | 31. R25 A28 |

# 5 Conclusions

One of the goals of the research was to find out why the amount of adherent anode slimes varies on the anode surface. This question could not be answered due to the fact that during sampling, the amount of adherent anode slimes was not documented. Other problems with the sampling were that the amount of some samples was too small to perform all of the analysis and that the samples were sometimes taken from one side of the anode and sometimes from both sides. In the future, a standard adherent anode slime amount documentation and sampling procedure should be used.

The analysis results show that, contrary to expectations, there is no clear correlation between the settling test results and the particle size distributions of the samples. This might be due to the fact that ultrasound was used to break up agglomerates in the particle size distribution measurements but not in the settling tests. With future samples, the particle size measurements could be first made without the ultrasound and perhaps with the ultrasound, after. Also, even though one particle size distribution measurement contained three repetitions, the measurements themselves should be repeated in order to assess the result reliability.

The chemical analysis show that, on average, silver has the highest and tellurium the lowest concentration in the adherent anode slimes. Nickel concentrations vary the most in the adherent anode slime samples and silver concentrations the least. The nickel concentration in the anodes and in the adherent anode slimes seems to have the best correlation and antimony the weakest. The concentrations of bismuth in the anodes and adherent anode slimes have a slight negative correlation. With the available chemical analysis methods, the concentration of oxygen could not be measured. According to the XRD analysis, $PbSO_4$ has a high score systematically in all of the adherent anode slime samples, which is in line with literature.

The chemical analysis results of the anode and adherent anode slime samples, together with the XRD analysis results seem to be in line with literature on the behavior of nickel in the anodes and anode slimes. However, the anode microstructures do not seem to confirm the presence of NiO. The SEM pictures taken of the adherent anode slimes did not reveal much.

In the identification of different adherent anode slime species, SEM EDS (Energy Dispersive Spectrometry) analysis might be a better technique in comparison to the XRD

measurements. The same SEM EDS analysis could also be used in the identification of different phases from the anode micrographs. In addition, at the current stage it is not possible to connect a certain anode with its chemical analysis. The problem is the same for the electrolyte analysis. In order to assess the factors affecting the adherent anode slimes, these connections should be made.

All in all, data of the adherent anode slimes could be produced. From this data, information can still be extracted in the form of detailed data correlation analysis. The process parameter data was not compared with the analysis results due to difficulties in connecting the sample with the corresponding data.

# 6 Summary

The goals of the thesis were to produce information of the adherent anode slimes and to examine the effects that anode composition and process parameters have on them. More specifically, a reason for the varying adherent anode slime amount and adherence was tried to be found. In literature, plenty of information was available of the electrorefining process, of copper anodes and of anode slimes. However, information of the adherence of the anode slimes was more rare and difficult to find.

In the experimental part, the adherent anode slime samples were examined with the help of moisture content determination, settling tests, particle size distribution measurements, chemical analysis, x-ray diffraction and scanning electron microscopy. Corresponding anode lug samples were examined with the help of chemical analysis and optical microscopy. The process parameter data was not compared with the analysis results due to difficulties in connecting the sample with the corresponding data.

From the produced analysis data, correlations were difficult to establish. However, a correlation was found between the chemical and XRD analysis results of nickel, which is also in line with literature. In the chemical analysis of the anode and adherent anode slime samples, the same samples had high nickel concentrations. In the XRD analysis, these same samples showed high scores of NiO and kupferglimmer.

The reason for the variation of anode slime amount and adherence on the anode surface could not be elucidated due to the fact that during sampling, the amount of the adherent anode slimes was not documented. Based on the analysis results, adherent anode slime sampling and some of the experimental methods need to be developed further. Also, information can still be extracted from the data produced, with the help of more advanced data analysis.

# References


Chen, T. T. & Dutrizac, J. E. 1989a. **A Minerological Study of the Deportment and Reaction of Silver during Copper Electrorefining**. Metallurgical Transactions B. Vol. 20B: June. Pp. 229-238. ISSN: 0360-2141 (print).

Chen, T. T. & Dutrizac, J. E. 1989b. **Minerological Characterization of Anode Slimes - IV. Copper-Nickel-Antimony Oxide ("Kupferglimmer") in CCR Anodes and Anode Slimes**. Canadian Metallurgical Quarterly. [Online publication]. Vol. 28:2. Pp. 127-134. [Time of reference: 19.5.2014]. Available at: `www.maneyonline.com/loi/cmq`. ISSN: 0008-4433 (print).

Chen, T. T. & Dutrizac, J. E. 1990a. **A Minerological Overview of the Behavior of Nickel during Copper Electrorefining**. Metallurgical Transactions B. Vol. 21B: April. Pp. 229-238. ISSN: 0360-2141 (print).

Chen, T. T. & Dutrizac, J. E. 1990b. **The Mineralogy of Copper Electrorefining**. Journal of Metals. Vol. 42:8. Pp. 39-44. ISSN: 1047-4838 (print).

Chen, T. T. & Dutrizac, J. E. 1991. **Mineralogical Characterization of Anode Slimes: Part 7 - Copper Anodes and Anode Slimes from the Chuquicamata Division of Codelco - Chile**. Canadian Metallurgical Quarterly. [Online publication]. Vol. 30:2. Pp. 95-106. [Time of reference: 31.10.2014]. Available at: `www.maneyonline.com/loi/cmq`. ISSN: 0008-4433 (print).

Chen, T. T. & Dutrizac, J. E. 1993. **The Minerological Characterization of Tellurium in Copper Anodes**. Metallurgical Transactions B. Vol. 24B: December. Pp. 997-1007. ISSN: 0360-2141 (print).

Cheng, W. & Hiskey, J. B. 1996. **Fundamental Studies of Copper Anode Passivation during Electrorefining: Part II. Surface Morphology**. Metallurgical and Materials Transactions B. Vol. 27B:4. Pp. 610-616. ISSN: 1073-5615 (print).

Davenport, W. G. & King, M. & Schlesinger, M. & Biswas, A. K. 2002. **Extractive Metallurgy of Copper**. 4th edition. Oxford, United Kingdom. ISBN: 0-08-044029-0 (print).

Demaerel, J. P. 1987. **The Behaviour of Arsenic in the Copper Electrorefining Process**.

In: Hoffman, J. E. & Bautista, R. G. & Ettel, V. A. & Kudryk, V. & Wesely, R. J. (eds.) The Electrorefining and Winning of Copper. Warrendale, Pennsylvania, USA. Pp. 195-210. ISBN: 0-87339-0580-X (print).

Forsén, O. 1985. **The behaviour of nickel and antimony in oxygen-bearing copper anodes in electrolytic refining**. Doctoral thesis. Helsinki University of Technology. Espoo, Finland. Pp. 90. ISBN: 951-753-648-1 (print).

Forsén, O. & Lilius, K. 1987. **Solidification and Electrolysis of Copper Anodes Containing Nickel, Arsenic, Antimony and Bismuth**. In: Hoffman, J. E. & Bautista, R. G. & Ettel, V. A. & Kudryk, V. & Wesely, R. J. (eds.) The Electrorefining and Winning of Copper. Warrendale, Pennsylvania, USA. Pp. 195-210. ISBN: 0-87339-0580-X (print).

Gu, Z. H. & Chen, J. & Fahidy, T. Z. 1995. **A study of anodic slime behaviour in the electrorefining of copper**. Hydrometallurgy. [Online publication]. Vol. 37:2. Pp. 129-147. [Time of Reference: 1.6.2014]. Available at: `www.sciencedirect.com/science/journal/0304386X/37/2`. ISSN: 0304-386X (online).

Krusmark, T. F. & Young, S. K. & Faro, J. L. 1995. **Impact of anode chemistry on high current density operation at Magma Copper's Electrolytic Refinery**. In: Cooper, W. C. & Dreisinger, D. B. & Dutrizac, J. E. & Hein, H. & Ugarte, G. (eds). Proceedings of COPPER 95-COBRE 95 International Conference, Volume III - Electrorefining and Hydrometallurgy of Copper. Montréal, Québec, Canada. Pp. 189-206. ISBN: 0-919086-64-0.

Larouche, P. 2001. **Minor Elements in Copper Smelting and Electrorefining**. Master's thesis. McGill University. Montreal, Canada. Pp. 165. ISBN: 0-612-79081-9.

Moats, M. S. & Hiskey, J. B. 2007. **The effect of Electrolyte Composition on Passivation of Commercial Copper Electrorefining Anodes**. In: Houlachi, G. E. & Edwards, J. D. & Robinson, T. G. (eds.) Proceedings of Copper 2007, Volume V, Copper Electrorefining and Electrowinning. Montréal, Québec, Canada. Pp. 47-58. ISBN: 1-894475-75-5 (print).

Moats, M. S. & Hiskey, J. B. 2010. **How Anodes Passivate in Copper Electrorefining**. In: GDMB (eds.) Proceedings of Copper 2010, Volume 4, Electrowinning and -refining. Clausthal-Zellerfeld, Germany. Pp. 1463-1482. ISBN: 978-3-940276-28-5 (print).

Moats, M. & Robinson, T. & Wang, S. & Filzwieser, A. & Siegmund, A. & Davenport, W. 2013. **Global Survey of Copper Electrorefining Operations and Practice**s. In: Abel, R. & Delgado, C. (eds.) Proceedings of Copper 2013, Volume V, Electrowinning / Electrorefining. Santiago, Chile. Pp. 307-318.

Moats, M. S. & Wang, S. & Kim, D. 2012. **A Review of the Behavior and Deportment of Lead, Bismuth, Antimony and Arsenic in Copper Electrorefining**. In: Wang, S. & Dutrizac, J. E. & Free, M. L. & Hwang, J. Y. & Kim, D. (eds.) T. T. Chen Honorary Symposium on Hydrometallurgy, Electrometallurgy and Materials Characterization. Hoboken, New Jersey, USA. Pp. 3-21. ISBN: 978-1-118-29123-8 (print).

Möller, C. A. & Friedrich, B. & Bayanmunkh, M. 2010. **Effect of As, Sb, Bi and Oxygen in Copper Anodes During Electrorefining**. In: GDMB (eds.) Proceedings of Copper 2010, Volume 4, Electrowinning and -refining. Clausthal-Zellerfeld, Germany. Pp. 1495-1510. ISBN: 978-3-940276-28-5 (print).

Schlesinger, M. E. & King, M. J. & Sole, K. C. & Davenport, W. G. 2011. **Extractive Metallurgy of Copper**. 5th edition. Oxford, United Kingdom. ISBN: 978-0-08-096789-9 (print).

Wang, X. & Chen, Q. & Yin, Z. & Wang, M. & Xiao, B. & Zhang, F. 2011. **Homogenous precipitation of As, Sb and Bi impurities in copper electrolyte during electrorefining**. Hydrometallurgy. [Online publication]. Vol. 105. Pp. 355-358. [Time of Reference: 6.6.2014]. Available at: `www.sciencedirect.com/science/journal/0304386X/`. ISSN: 0304-386X (online).